B Seismic investigations (receiver functions)

The Moho depth and morphology is one of the most important features to characterize the overall structure of the lithosphere, i.e. it is a key for the reconstruction of the tectonic evolution of the region. The depth variations of the discontinuities bounding the mantle transition zone at about 410 km and 660 km depths (‘410’ and ‘660’) are also important to characterize the (physical/chemical) properties of the upper mantle and the mantle transition zone.

The receiver function method is an excellent tool for detecting seismic discontinuities (e.g., Moho) within the lithosphere and the deeper upper mantle analysing Ps conversions [*Vinnik,* 1977; *Langston,* 1979; *Zandt et al.,* 1995]. The fundamentals of the method are described, e.g., by *Kind and Vinnik* [1988] and *Kind et al.* [1995]. The method allows the evaluation of crustal and mantle structures at regional scales (plumes, subduction zones, and continental plate boundaries). Case studies demonstrate the high scientific potential of the receiver function method: Hawaiian and other oceanic mantle plumes [*Li et al.,* 2000a, 2003a], Japan and Hellenic subduction zones [*Li et al.,* 2000b, 2003b], Central Andes [*Yuan et al.,* 2000, 2002], detached Indian lithospheric mantle beneath Tibet [*Kosarev et al.,* 1999; *Kind et al.,* 2002], and the structure of the continental plate boundary between the Baltic Shield and the German-Polish Basin in Europe [*Gossler et al.,* 1999; *Alinaghi et al.,* 2003]. P-SV conversions also provide evidence for a magma chamber beneath the Campi Flegrei Caldera near Naples, Italy [*Ferrucci et al.,* 1992].

B.1 Observational technique (receiver function method)

The basis of the receiver function analysis is three-component recording of teleseismic events. P-to-S conversions at seismic discontinuities are caused by incident P-waves being partly converted to S-waves. These phases travel their last leg with shear wave velocity and arrive in the coda of the P-wave on the radial component, consequently. Amplitudes, arrival times, and polarity of the Ps-phases are mainly sensitive to the shear wave velocity distribution beneath the recording site. These converted phases can be extracted from the P-coda applying several processing steps, including rotation into the ray co-ordinate system of the P-, SV- and SH components, restitution of broadband ground displacement, deconvolution in time domain to remove the source time function and travel path effects [e.g., *Kind et al.,* 1995], distance move-out (time) corrections for a reference epicentral distance of 67° [*Yuan et al.,* 1997], and stacking. The processed receiver functions provide images of the crust and upper mantle similar to steep angle reflection images of the crust. The seismic wave periods used (one to several seconds; strongly depending on the instruments used and noise conditions) are longer than in controlled source seismic measurements, because teleseismic earthquakes are utilized as sources.

Also, multiple reflections and conversions between the base of the crust and the surface of the Earth occur and must be considered (Figure B.1). For the calculations of move-out corrections and the Moho piercing point locations, the IASP91 seismic velocity model [*Kennett*, 1991; *Kennett and Engdahl,* 1991] was used.

The depth of the Moho and the average crustal v_p/v_s ratio were computed using the method of *Zhu and Kanamori* [2000], which considers besides the direct conversion from the Moho, also its multiples. *Zandt et al.* [1995] and *Zandt and Ammon* [1995] used a similar approach. A grid search for the maximum-stacked amplitude in the Moho depth (H) versus v_p/v_s domain was carried out in the interval of 20 to 60 km depth and 1.5 to 2.0 for the v_p/v_s ratio. Because the multiple phases have nearly identical curves in the H-v_p/v_s domain and sample a broader area, primary phases and the two multiple conversions were weighted before stacking with the values 0.5, 0.25 and 0.25, respectively, according to the suggestions of *Zhu and Kanamori* [2000].

To get an idea of the response of crustal structure in the investigated area, synthetic receiver functions were calculated for published seismic velocity models from the western and northern Bohemian Massif (see Figure B.10, below) using the approach of *Kind et al.* [1995]. They assumed that the Earth's crust could be modelled as a stack of horizontal homogenous layers over a homogeneous half-space. The incoming P-wave is considered to be a plane wave with a specific apparent velocity. *Kind et al.* [1995] showed that there are only small differences in the results using plane waves or reflectivity theoretical seismograms.

B.2 Data

In this study, teleseismic data from broadband and short-period seismological stations of several temporary networks, operated by the Seismologisches Zentralobservatorium Gräfenberg (SZGRF), the GeoForschungsZentrum Potsdam (GFZ), the Dublin Institute for Advanced Studies (DIAS), and the Universities of Munich, Potsdam and Stuttgart, and permanent networks of SZGRF, GRSN (German Regional Seismic Network), and the Institute of Geophysics, Praha of the Czech Academy of Sciences (IG CAS), were analysed (Figure B.2). Furthermore, the data from two permanent short-period seismic networks in NW-Bohemia (Figure B.2b), the WEBNET of IG CAS and the KRASNET of the Institute of Physics of the Earth, Brno (IPE Brno), were studied. More details are given in Tables B.I and B.II. The stations equipped with MARK (1s) seismometers (Table B.I) were restituted up to 12 seconds and are further referred as broadband stations. Almost all stations in the central study area (northeast of the Franconian Lineament) are grounded on crystalline rocks.

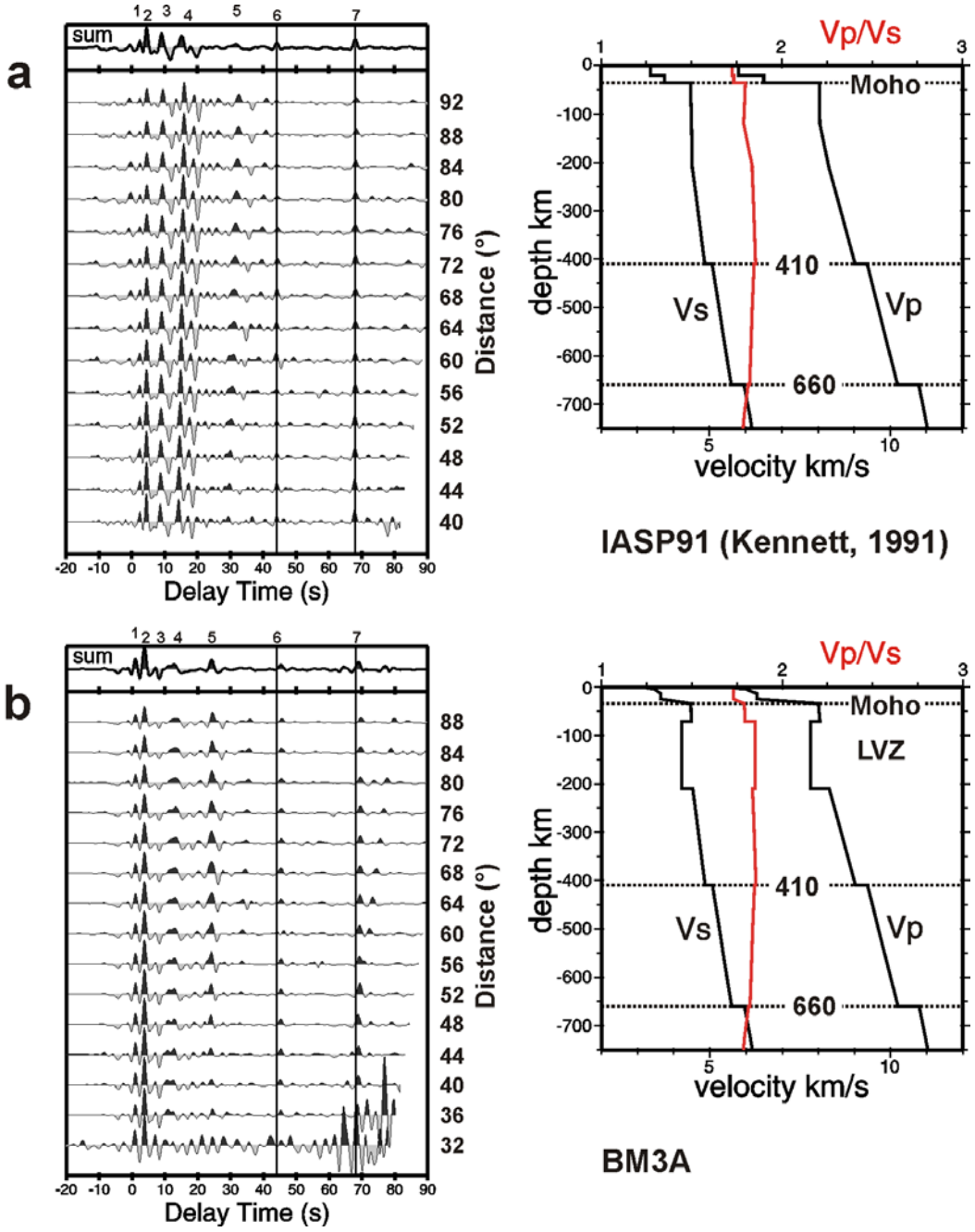

Figure B.1
Synthetic receiver functions from reflectivity theoretical seismograms [reflectivity method of *Kind*, 1985] calculated for **(a)** the IASP91 velocity model [*Kennett and Engdahl,* 1991] and **(b)** a hypothetic regional velocity model incorporating an asthenospheric low-velocity zone (LVZ; 71 to 210 km depth), which is missing in the IASP91 reference model. The source was presumed near the surface. The seismic velocity structure is the same at the source and receiver sides. Synthetic seismograms were processed like the natural data. Move-out corrected receiver functions are shown for different epicentral distances.
Converted (primary and multiple) phases are clearly visible within the first 20 seconds delay time, which stem from the Moho (2, 4) and crustal discontinuities (1, 3 for IASP91). Phases (5) around 30 seconds delay time for the IASP91 model **(a)** might represent further multiple phases from the crust, whereas the phase (5) visible in **(b)** stem from the sharp base of the hypothetical upper mantle low-velocity layer. The conversion from the upper boundary of the low-velocity layer is visible as a minimum at 8 seconds delay time (3). But in natural data it might be difficult to detect it due to interferences with the Moho conversion and crustal multiples.
Vertical solid lines at about 44.1 and 68.1 seconds delay time mark the delay times of converted phases from the discontinuities of the mantle transition zone (‘410’ and ‘660’), according to the IASP91 velocity model. As expected, the modelled conversions (6, 7) in **(a)** fit the theoretical delay time, whereas converted phases in model **(b)** arrive later than predicted by the IASP91 reference model (45.4 and 68.9 seconds delay time).

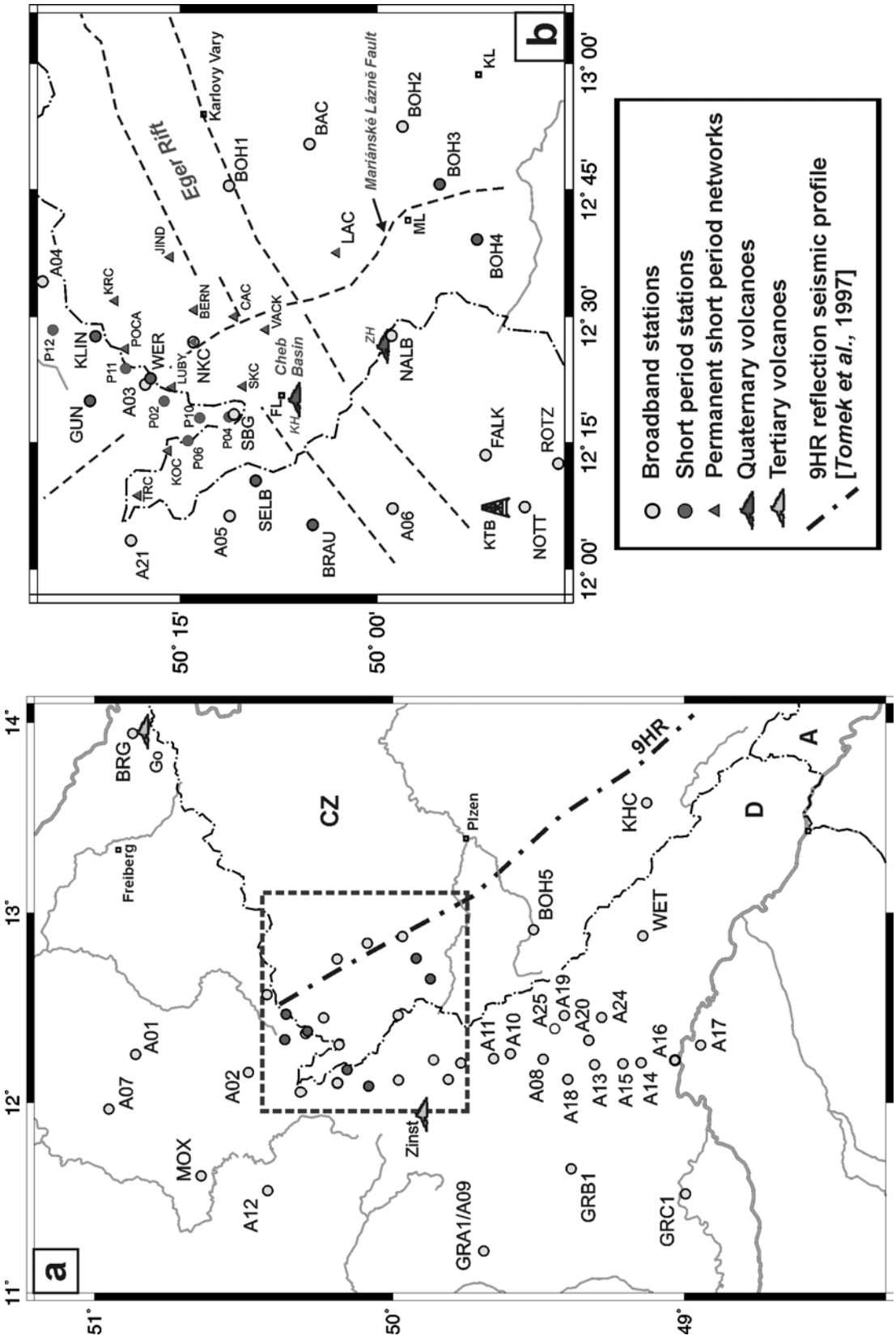

Figure B.2
(a) Distribution of the seismological stations in the western Bohemian Massif, from which data are used in this study. Also shown are the xenolith sample sites Gottleuba (Go) and Zinst. **(b)** Enlarged map of the Vogtland/NW-Bohemia region with the locations of all short period and broadband stations, the 9HR reflection seismic profile [*Tomek et al.,* 1997], main faults (hatched lines), and the Quaternary scoria cones.
KTB – location of the German Continental Deep Drilling Boreholes (KTB), FL – Františkovy Lázně, ML – Mariánské Lázně, KL – Konstantinovy Lázně, KV – Karlovy Vary, KH – Komorní Hůrka, ZH – Železná Hůrka.

Seismic events within an epicentral distance range from 30° to 97° and magnitudes > 5.5 were analysed. Only events with a good signal-to-noise-ratio of the P-onset and without disturbances within 100 seconds after the P-onset were selected. The theoretical back-azimuth angle was used for rotation, whereas the incidence angle was generally computed from the waveforms of the radial and vertical components.

B.3 Results

B.3.1 Observed receiver functions (single and sum traces)

Good observations of the Moho conversions and the crustal multiples were made at about 50 stations in the region under study (Figures B.3, B.4). Most stations of the KRASNET and WEBNET networks (Figure B.5) yielded also good Moho conversions, in spite of their short period seismometers and the short recording windows (triggered operation mode). Finally, also the short-period stations of the temporary deployment during the earthquake swarm 2000 yielded acceptable receiver functions, but the number of analysed events is strongly limited (Figure B.5).

At some stations, positive Ps-phases originating in the upper crust within 2 seconds after the P-onset were observed. Most of the crustal arrivals are related to strong velocity gradients, which exist in the uppermost crystalline crust [*Malek et al*., 2001; *Hemmann et al.*, 2003] or a sedimentary cover (e.g., stations GRA1, GRB1, GRC1, FUR). Receiver function modelling of published velocity models confirms these effects of the uppermost kilometres (see Figure B.10). Later Ps conversions within 3 seconds delay time might be caused by deeper structures like the “Erbendorf body” (*DEKORP Research Group*, 1988; *Schmoll et al.,* 1989) beneath the station NOTT. Deeper crustal arrivals were also observed at the short-period stations SKC, CAC and LAC (Figure B.5).

At almost all stations strong conversions with positive polarity (indicating velocity increase downwards) with delay times of about 3.6 seconds after the P-wave can be seen in single traces (Figure B.3) as well as in the stacked traces (Figures B.4 and B.5). These conversions can be attributed to the Moho discontinuity. Moho multiples are visible in Figures B.3 and B.4 near 13 seconds (positive, PpPs) and 16 seconds (negative, PpSs+PsPs). These multiples are weaker or do not exist in Figure B.5 because only short-period stations are displayed there. Multiples loose higher frequencies when travelling two times more through the attenuating and scattering crust. At station NKC, a distortion of the Moho multiples is visible in traces from southeastern to western azimuths, whereas only a slight anomaly exists in the direct Moho conversions. This might be an indication for an anomaly at the crust-mantle boundary 10 to 20 km away from the station.

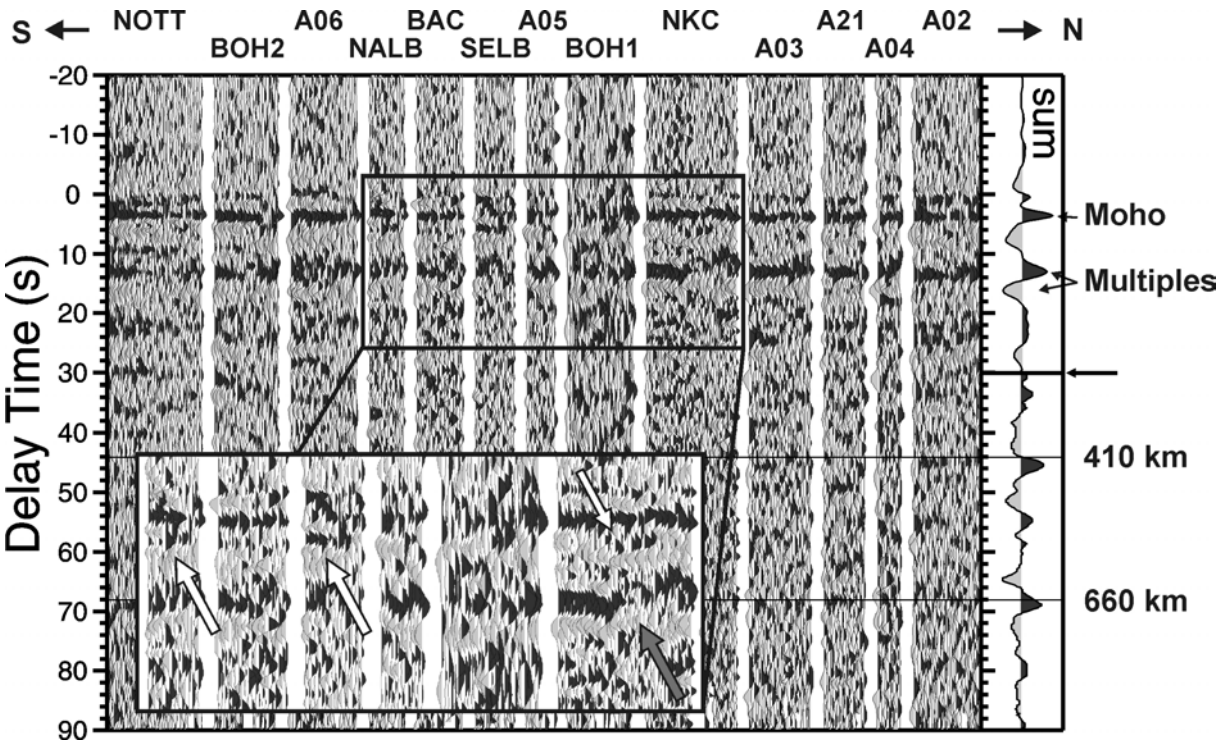

Figure B.3
Individual receiver functions for some stations within the region shown in Figure B.2b. Traces were high-pass filtered with 12 seconds corner period and move-out corrected. A delay time of 0 second is equivalent to the P-wave arrival time. Traces were clock-wise sorted after back-azimuth for each station (from left to right).
The average delay time for P-to-S converted waves from the Moho discontinuity is about 3.6 seconds. Multiple phases from the Moho arrive with about 13 and 16 seconds delay time. At station NKC, a distortion of the Moho multiples is visible in traces from southeastern to western azimuths (to the right of the dark grey arrow), whereas there are only slight variations in the direct Moho conversions. Additional phases with 6 seconds delay time are visible at the stations SELB, NALB and NKC (light arrows). The conversions from the upper mantle discontinuities at 410 km and 660 km depth can be seen in the stack trace. The amplitudes are four times enlarged in the delay time window from 30 to 90 seconds (arrow: change in scale). Both Ps phases arrive later as predicted by the IASP91 velocity model [straight lines; *Kennett and Engdahl*, 1991], possibly indicating lower seismic velocities above the 410 km discontinuity than in the IASP91 velocity model.

Additionally, conversions are observed at about 6 to 9 seconds delay time at some stations. Especially interesting is a phase near 6 seconds delay time beneath the region of earthquake swarms, which is detectable beneath several stations in this area (stations SELB, NALB, and NKC in Figure B.3). Stacking the single traces with move-out corrections for primary and multiple phases implies that the observed “6 s phase” might be a primary one, however the move-out differences are very small and are within the resolution limits.

Signals from 410 and 660 km discontinuities are delayed by up to 2 seconds compared to theoretical delay times calculated from the IASP91 reference model (sum trace in Figure B.3). This could be an indication for reduced seismic velocities in the upper mantle (above 410 km) relative to the reference earth model. Further results and discussion dealing with the mantle transition zone discontinuities follow below in section B.3.4.

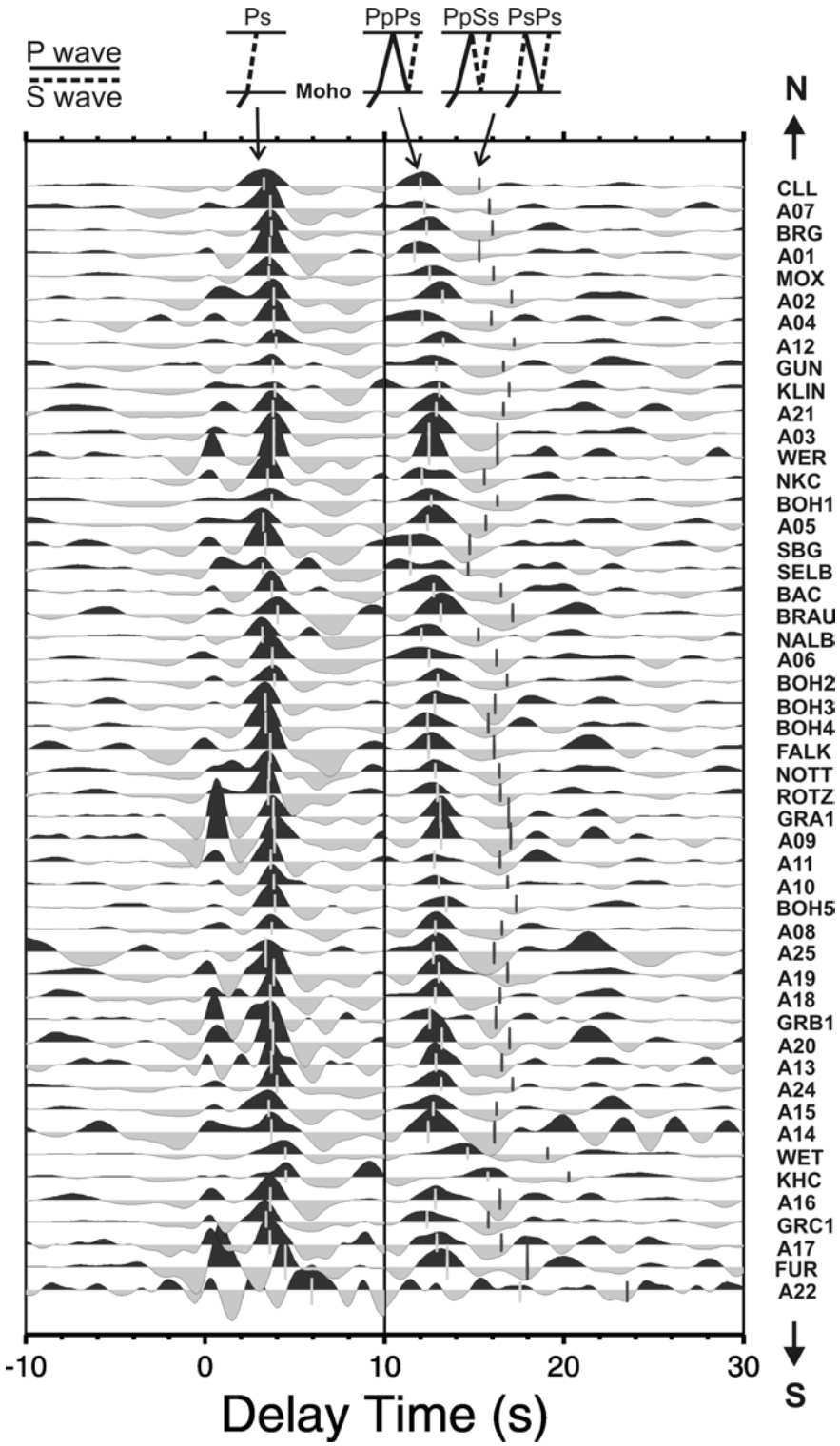

Figure B.4
Stacked receiver functions from broadband stations, aligned from the north (top) to the south (bottom). Traces were high-pass filtered with 12 seconds corner period and move-out corrected for primary Ps (-10 to 10 seconds delay time) and multiple PpPs (10 to 30 seconds delay time) conversions before stacking. The average delay time for P-to-S converted waves from the Moho discontinuity is about 3.6 seconds. Multiple phases (PpPs and PpSs+PsPs) from the Moho arrive with about 13 and 16 seconds delay time. Re-calculated delay times of the direct Ps-converted phase and its multiples from the Moho are marked, using the Moho depths and v_p/v_s ratios from Table B.1 and an average crustal P-wave velocity of 6.3 km/s.
Stations CLL, FUR, and A22 are situated outside the area shown in Figure B.2a. The deepening of the Moho towards the Alps can be seen at station A22 (near Innsbruck, Austria).

Table B.I. Seismological station parameters (including station code, latitude, longitude, elevation, operating institutions, recording time, and seismometer type) for broadband instruments, crustal thickness (H_c), crustal v_p/v_s ratio, Ps delay times (t_{ps}) for the Moho, '410' and '660' discontinuities, and number of stacked traces (n).
The data were band-pass filtered using different corner periods for the analyses of the Moho (temporary stations: 1 to 12 seconds; permanent stations: 1 to 20 seconds) and '410'/'660' (temporary stations: 5 to 20 seconds; permanent stations 5 to 50 seconds) discontinuities, respectively. Different numbers n belong to the analyses for the Moho and the mantle transition zone discontinuities, respectively.

Station	Lat [°E]	Lon [°N]	Elev. [m]	Institution	Data	Seismometer	H_c [km]	v_p/v_s	t_{ps}[s] Moho	t_{ps}[s] 410	t_{ps}[s] 660	n
CLL	13.003	51.308	230	GRSN	1993 - 1997	STS-2	29.5±2.0	1.67±0.11	3.3	43.3	67.7	180/230
BRG	13.943	50.873	296	GRSN	1993 - 1997	STS-2	29.3±1.8	1.76±0.08	3.6	44.8	68.4	177/210
MOX	11.656	50.645	455	GRSN	1992 - 1997	STS-2	30.3±1.8	1.71±0.07	3.5	44.0	68.0	193/228
TNS	8.449	50.224	815	GRSN	1991 - 1997	STS-2	24.5±2.0	1.74±0.11	2.8	45.6	69.5	236/272
WET	12.878	49.144	613	GRSN	1991 - 1997	STS-2	34.3±1.8	1.79±0.09	4.4	45.3	68.6	249/298
STU	9.190	48.770	360	Stuttgart/GEOFON	1996 - 2003	STS-2	24.8±2.3	1.73±0.11	2.9	44.6	67.8	54/354
BFO	8.330	48.331	589	GRSN	1991 - 1997	STS-2	27.0±1.5	1.67±0.10	2.9	44.0	68.1	219/277
FUR	11.277	48.164	565	GRSN	1991 - 1997	STS-2	30.5±1.5	1.89±0.06	4.3	44.3	68.1	236/282
GRA1	11.222	49.692	500	SZGRF	1980 - 1997	STS-1	31.5±0.5	1.73±0.05	3.7	45.7	68.7	397/694
GRB1	11.652	49.391	494	SZGRF	1980 - 1997	STS-1	29.8±1.3	1.75±0.06	3.6	44.5	68.3	349/622
GRC1	11.521	48.996	512	SZGRF	1980 - 1997	STS-1	30.3±1.8	1.68±0.07	3.3	43.9	68.8	325/587
NKC	12.361	50.233	564	IG CAS	2000 - 2003	STS-2	28.8±1.8	1.73±0.07	3.4	47.7	69.3	89
DPC	16.322	50.350	784	IG CAS	2000 - 2003	STS-2	27.8±1.3	1.80±0.08	3.7	44.5	69.1	144
PRU	14.542	49.988	302	IG CAS	2000 - 2003	CMG-3T	33.0±1.0	1.67±0.05	3.6	45.4	70.6	107
KHC	13.578	49.131	700	IG CAS	2000 - 2003	STS-2	38.3±1.8	1.71±0.05	4.5	44.8	68.7	156
BOH1*	12.757	50.188	420	GFZ/SZGRF	1997- 2001	40T/ MARK/ TSJ	30.0±1.5	1.75±0.10	3.6	45.8	68.5	30/13
BOH2*	12.874	49.967	660	GFZ/SZGRF	1997 - 1998	GURALP-40T	30.8±1.8	1.76±0.09	3.8	45.3	68.6	36
BOH3	12.760	49.920	610	GFZ/SZGRF	1997 - 1998	MARK-L-4-3D	32.0±1.5	1.63±0.07	3.3	45.9	69.1	15
BOH4	12.651	49.872	605	GFZ/SZGRF	1997 - 1998	MARK-L-4-3D	30.5±1.5	1.67±0.07	3.3	45.2	69.6	21
BOH5*	12.000	49.520	380?	GFZ/SZGRF	1997 - 1998	GURALP-40T	32.3±1.8	1.73±0.07	3.8	45.4	69.0	30
NOTT	12.910	49.811	490	KTB/Munich	1995	STS-2	31.3±1.3	1.69±0.05	3.5	46.3	69.2	42/44
FALK	12.225	49.861	465	KTB/Munich	1995	STS-2	29.8±1.8	1.74±0.07	3.6	45.8	68.1	12
ROTZ	12.208	49.768	430	KTB/Munich	1995	STS-2	31.8±1.3	1.67±0.05	3.5	46.0	70.0	18/16
A01	12.255	50.863	270	GFZ/SZGRF	1995 - 1996	GURALP-3T	27.3±1.8	1.80±0.08	3.5	48.0	68.8	26
A02	12.159	50.487	414	GFZ/SZGRF	1995 - 1996	GURALP-3T	31.8±1.3	1.72±0.08	3.8	45.5	67.1	30
A03	12.364	50.294	670?	GFZ/SZGRF	1995 - 1996	GURALP-3T	29.3±1.3	1.79±0.07	3.8	44.7	49.6	28/27
A04	12.568	50.424	915?	GFZ/SZGRF	1995 - 1996	STS-2	28.0±1.5	1.81±0.11	3.8	44.7	67.1	9

* GURALP-40T seismometers were provided by the Dublin Institute for Advanced Studies (DIAS).

Table B.I. (continued).

Station	Lat [°E]	Lon [°N]	Elev. [m]	Institution	Data	Seismometer	H_c [km]	v_p/v_s	t_{ps}[s] Moho	t_{ps}[s] 410	t_{ps}[s] 660	n
A05	12.104	50.187	670	GFZ/SZGRF	1995 - 1996	3T/MARK	29.5±1.5	1.68±0.08	3.4	(50.4)	(66.9)	22
A06	12.119	49.980	635	GFZ/SZGRF	1995 - 1996	GURALP-3T	29.5±2.0	1.77±0.09	3.6	45.5	71.0	30
A07	11.967	50.952		GFZ/SZGRF	1995 - 1996	GURALP-3T	29.0±2.0	1.76±0.08	3.5	44.9	68.4	20
A08	12.229	49.487	469	GFZ/SZGRF	1995 - 1996	GURALP-3T	30.8±1.3	1.73±0.07	3.7	45.4	68.5	19
A09	11.222	49.692	499	GFZ/SZGRF	1995 - 1996	STS-2	31.5±1.0	1.74±0.06	3.9	46.0	67.5	15
A10	12.258	49.599	597	GFZ/SZGRF	1995 - 1996	GURALP-3T	31.0±1.0	1.75±0.05	3.7	46.3	66.4	17
A11	12.233	49.656	665	GFZ/SZGRF	1995 - 1996	STS-2	30.8±1.8	1.72±0.06	3.6	46.1	68.8	29
A12	11.538	50.422		GFZ/SZGRF	1995 - 1996	STS-2	31.5±1.5	1.76±0.08	3.9	45.3	69.1	28
A13	12.200	49.311	448	GFZ/SZGRF	1995 - 1996	STS-2	31.0±1.0	1.72±0.05	3.6	46.5	68.1	10
A14	12.211	49.150	512	GFZ/SZGRF	1995 - 1996	STS-2	29.3±1.8	1.76±0.08	3.7	(47.8)	(68.9)	2
A15	12.205	49.213	428	GFZ/SZGRF	1995 - 1996	STS-2	31.0±1.5	1.69±0.08	3.5	44.5	68.1	28
A16	12.224	49.033		GFZ/SZGRF	1995 - 1996	STS-2	31.0±1.5	1.71±0.08	3.6	45.1	69.4	22
A17	12.303	48.944	212	GFZ/SZGRF	1995 - 1996	STS-2	31.5±1.5	1.69±0.06	3.5	44.5	67.4	19
A18	12.122	49.402	360	GFZ/SZGRF	1995 - 1996	STS-2	31.0±1.0	1.71±0.06	3.6	45.2	69.8	16
A19*	12.459	49.414		GFZ/SZGRF	1995 - 1996	GURALP-40T	31.0±1.5	1.75±0.07	3.8	44.2	69.3	17
A20	12.328	49.330	475	GFZ/SZGRF	1995 - 1996	STS-2	31.8±1.3	1.72±0.06	3.7	46.7	66.9	9
A21	12.056	50.312		GFZ/SZGRF	1995 - 1996	GURALP-3T	30.8±1.3	1.74±0.07	3.7	48.5	68.5/72.4	19
A22	11.300	47.150		GFZ/SZGRF	1995 - 1996	STS-2	39.3±2.8	1.92±0.11	6.0	(47.7)	(67.9/72.0)	7
A24	12.449	49.286	555	GFZ/SZGRF	1995 - 1996	GURALP-3T	31.0±1.5	1.78±0.08	3.9	47.5	69.0	13
A25*	12.389	49.447	555	GFZ/SZGRF	1995 - 1996	GURALP-40T	31.5±2.0	1.65±0.10	3.4	-	-	3
WER	12.376	50.287	780	GFZ/SZGRF	1999 - 2000	MARK-L-4-3D	29.3±1.3	1.79±0.08	3.7	(49.5)	(69.2)	10
GUN	12.332	50.364	708	GFZ/SZGRF	1999 - 2000	MARK/TSJ-10	30.8±1.8	1.74±0.07	3.7	(49.1)	(68.2)	14/7
KLIN	12.462	50.358	640	GFZ/SZGRF	1999 - 2001	MARK-L-4-3D	31.0±1.0	1.76±0.06	3.8	-	-	21
SELB	12.179	50.154	580	GFZ/SZGRF	1999 - 2001	MARK/ TSJ-10	27.8±1.3	1.70±0.06	3.1	45.5	67.7	18/14
NALB	12.461	49.981	660	GFZ/SZGRF	2000 - 2001	MARK/STS2/TSJ	30.0±1.5	1.64±0.06	3.1	47.4	69.3	16/17
BAC	12.840	50.086	530	GFZ/SZGRF	2000 - 2001	TSJ-10	30.5±1.0	1.74±0.06	3.7	45.9	69.6	21
SBG	12.305	50.182	595	GFZ/SZGRF	1998 - 2001	TSJ-10	27.3±2.3	1.74±0.11	3.2	(45.8)	(67.4)	5
BRAU	12.087	50.082	600?	GFZ/SZGRF	1998 - 1999	MARK-L-4-3D	30.8±1.8	1.79±0.11	4.0	-	-	7
						Average:	30.5±1.5	1.73±0.08	3.6			

* GURALP-40T seismometers were provided by the Dublin Institute for Advanced Studies (DIAS).

Table B.II. Same as in Table B.I for short-period networks (except of Ps delay times for the '410' and '660'). v_p/v_s ratios were taken from nearby broadband stations to calculate crustal thickness from Moho Ps dealy time (t_{Ps}).

Station	Lat [°E]	Lon [°N]	Elev. [m]	Institution	Data	Seismometer	H_c [km]	v_p/v_s	t_{ps}[s]	n
POCA	12.435	50.319	800	IPE Brno	1997 - 1998	WDS	30.7	1.77	3.9	29
LUBY	12.359	50.260	625	IPE Brno	1997 - 1998	WDS	28.0	1.78	3.6	31
JIND	12.617	50.262	722	IPE Brno	1997 - 1998	WDS	28.3	1.75	3.5	15
BERN	12.512	50.232	635	IPE Brno	1997 - 1998	WDS	29.9	1.73	3.6	20
TRC	12.151	50.310	566	IG CAS	1997 - 1998	SM-3?	31.1	1.74	3.8	40
KOC	12.234	50.265	575	IG CAS	1997 - 1998	SM-3	31.9	1.74	3.9	50
KRC	12.530	50.332	760	IG CAS	1997 - 1998	SM-3	27.1	1.76	3.4	53
NKC	12.448	50.233	564	IG CAS	1997 - 1998		29.0	1.73	3.5	54
CAC	12.499	50.181	578	IG CAS	1997 - 1998	SM-3?	29.5	1.74	3.6	11
SKC	12.361	50.170	455	IG CAS	1997 - 1998	LE-3D	28.6	1.74	3.5	16
LAC	12.514	49.967	838	IG CAS	1997 - 1998	SM-3	28.6	1.74	3.5	44
P02	12.396	50.319		Uni Potsdam/GFZ	2000	LEN5s/MARK	28.8	1.78	3.7	3
P04	12.300	50.188		Uni Potsdam/GFZ	2000	LEN5s/MARK	27.0	1.74	3.3	6
P06	12.253	50.240		Uni Potsdam/GFZ	2000	LEN5s/MARK	23.7	1.74	2.9	9
P10	12.298	50.225		Uni Potsdam/GFZ	2000	LEN5s/MARK	25.4	1.74	3.1	3
P11	12.331	50.270		Uni Potsdam/GFZ	2000	LEN5s/MARK	28.6	1.74	3.5	7
P12	12.472	50.411	825?	Uni Potsdam/GFZ	2000	LEN5s/MARK	31.1	1.74	3.8	8
						Average:	28.7	1.75	3.5	

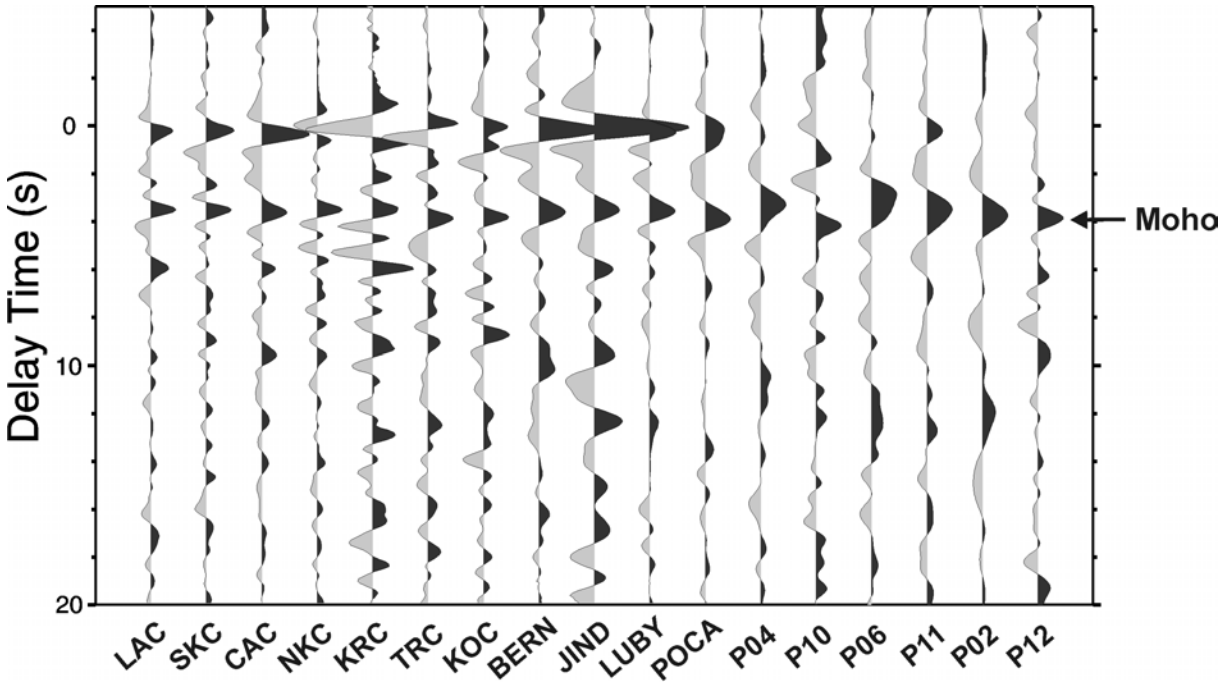

Figure B.5
Stacked receiver functions from short-period stations. Integration was applied instead of the usual restitution of ground displacement before the traces were high-pass filtered with 5 seconds corner period. Conversions at the Moho are observed, whereas short period instruments did not allow the identification of multiple phases.

There are also positive phases visible in the sum traces at individual stations at about 20 seconds delay time, but they are not very coherent from station to station. These phases might be a hint for a discontinuity near 220 km depth as proposed in the PREM-model [*Dziewonski and Anderson,* 1981]. Generally, Ps conversions from the 220 km discontinuity interfere with crustal multiples, and they are therefore difficult to detect using Ps receiver functions [see *Kind and Vinnik,* 1988].

B.3.2 Moho depth

To compute the Moho depth (crustal thickness) and v_p/v_s ratios, the data were stacked using a method introduced by *Zhu and Kanamori* [2000] (Table B.I and Figure B.6). In Figure B.7a-c the observed Moho Ps delay times, Moho depths, and v_p/v_s ratios from all broadband stations and stations with MARK-L-4-3D seismometers in the region were mapped. The corresponding values are given in Table B.I. To a first approximation, the map of Ps delay times (Figure B.7a) can be regarded as an initial Moho map assuming a constant v_p/v_s ratio of 1.73 for all stations and multiplying the recorded delay times by an empirical value of 8.4 km/s. Obviously most of the region has delay times of about 3.7 seconds (green dots, about 31 km depth). In the Vogtland/NW-Bohemia region and the area near the station GRC1, the converted phases from the Moho arrive 3.0 to 3.3 seconds after the P-wave (reddish dots, 25 to 28 km depth). Later arrivals (4.3 to 4.5 seconds delay time, blue dots, 36 to 38 km depth) are observed at the stations WET and KHC in the southeast of the area under study.

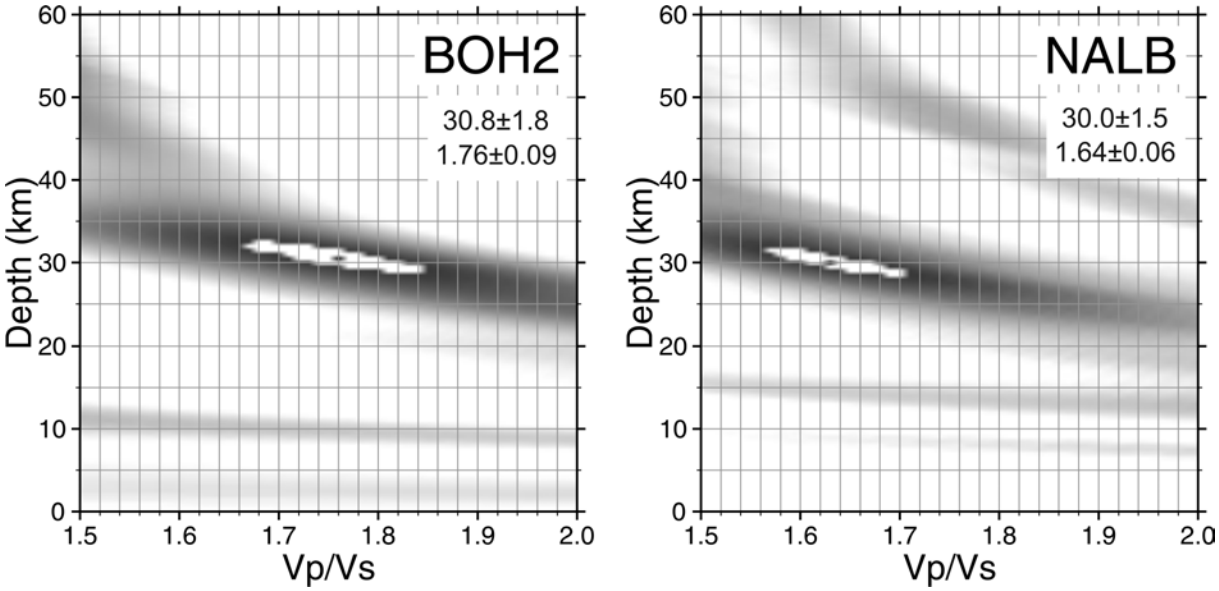

Figure B.6
Inversion results of Moho depth versus v_p/v_s ratio for the stations BOH2 and NALB. The maximum stacked amplitudes were found by grid search within the intervals of 20 to 60 km for the Moho depth and 1.50 to 2.00 for the v_p/v_s ratio. An average crustal P-wave velocity of 6.3 km/s was assumed. The surrounding white area marks the region of 95 % of the maximum stacked amplitude. The half-width of the 95 %-region gives an estimate of the uncertainty of the method.

Figure B.7 (next page)
(a) Map of Moho conversion times (Ps delay times, Table B.I) for the broadband stations. The mean value for all stacked traces at a specific station is projected onto the piercing points of rays at Moho level (30 km depth). This shows the back-azimuth coverage at each station. As can be expected, the permanent observatories have better back-azimuth coverage than temporary stations with only a few months of registration time. **(b)** Map of Moho depths and **(c)** map of v_p/v_s ratios compiled on the basis of the results of the inversion method proposed by *Zhu and Kanamori* [2000] (see Table B.I; assuming an average crustal P-wave velocity of 6.3 km/s).

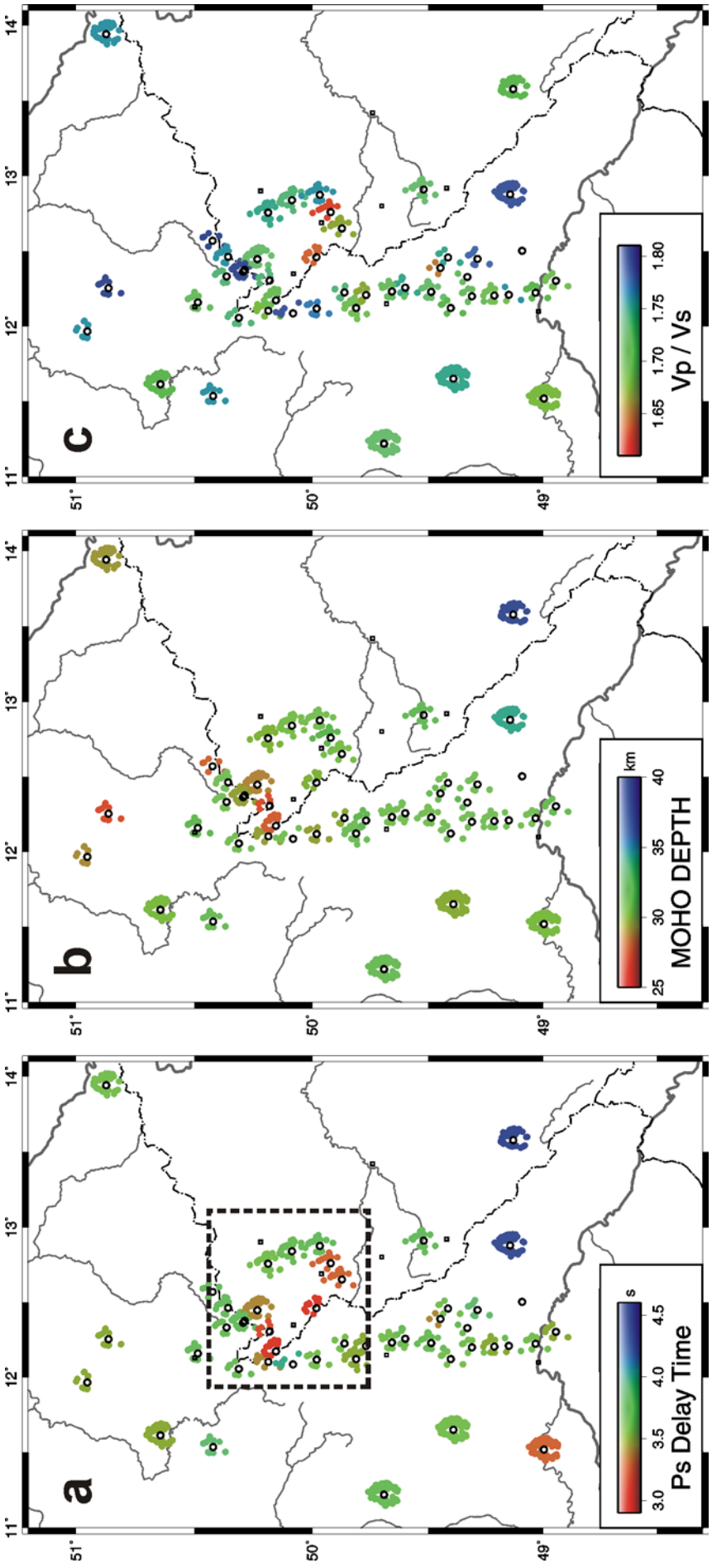
a
Ps Delay Time
s
3.0
3.5
4.0
4.5
b
MOHO DEPTH
km
25
30
35
40
c
Vp / Vs
1.65
1.70
1.75
1.80
11°
12°
13°
14°
49°
50°
51°

The results from the receiver function analysis after *Zhu and Kanamori* [2000] were compiled into a map of Moho depths (crustal thicknesses) for the region NW-Bohemia/NE-Bavaria/Vogtland (Figure B.7b). This map is not corrected for the station elevation. In general, the Moho depth increases from NW (31 km) to SE (38 km). Beneath the Cheb Basin the Moho seems to dome up to at least 27 to 28 km. However, this anomaly does not reach as far south as the Ps delay time anomaly in Figure B.7a. Moho depths of about 27 to 28 km were also obtained further north (station A01). The area around GRC1 shows no Moho depth anomaly as in the Ps delay times. This is due to a decreased v_p/v_s ratio (see Figure B.7c). Stations WET and KHC in the SE show the deepest Moho (34 and 38 km). Generally, the observed Moho depths are in good agreement with values obtained by several regional refraction and reflection seismic studies.

B.3.3 Crustal v_p/v_s ratios

A map of the v_p/v_s ratios (Figure B.7c) was compiled from the inversion results listed in Table B.I. The average value in the region is 1.73. Higher v_p/v_s ratios (1.76-1.81) are measured beneath the western Erzgebirge Mountains (stations A03, A04, WER). Decreased values (1.63-1.69) are obtained beneath the German-Czech border region east of the KTB (stations NALB, BOH3, BOH4), the southern KTB-area (stations NOTT, ROTZ), and north and west of Regensburg (stations A15, GRC1). Very high values of 1.89 were measured beneath the Molasse Basin and the northern Alps (stations FUR and A22, not on the map). The discrepancy between different Moho depths and nearly identical Moho Ps delay times at the two CO_2 emanation centres, FL (Františkovy Lázně / Cheb Basin; stations SELB, SBG) and ML (Mariánské Lázně; stations BOH3, BOH4), is associated with the observation of lower v_p/v_s ratios in the more southern area. Similar observations were also made in other areas worldwide [e.g., *Yuan et al.,* 2002].

There exist several possibilities to explain such relatively low values, which seem to be very low compared to laboratory measurements of typical crystalline crustal rocks. *Christensen* [1996] estimated an average v_p/v_s ratio for the continental crust of about 1.76 from laboratory measurements of typical crustal rocks. Values < 1.65 were only measured for rocks with high quartz content. Another possibility to explain low values is the presence of fluids under normal pore pressure within pores of low aspect ratio [*Lüschen et al.,* 1993]. Recently published seismic velocity models for the upper crust of NW-Bohemia [e.g., *Janský et al.,* 2000; *Málek et al.,* 2000] also show relatively low v_p/v_s ratios. Possibly, the low v_p/v_s ratios observed for the upper crust are valid for the whole crust in distinct parts of the regions. Maybe quartz-rich rocks or the presence of fluids dominate these parts.

Generally, a sedimentary cover containing layers with very low shear wave velocities could influence the distribution of v_p/v_s ratios, but almost all stations in this study are grounded on crystalline rocks.

Some stations in the southwestern study area (GRA1, GRB1, GRC1, A13, and A17) are installed on sedimentary rocks, up to approximately 1200 m thick [see *Krüger and Weber,* 1992]. However, this thin sedimentary cover should not have a huge influence on the average crustal v_p/v_s ratio. High v_p/v_s ratios at the southernmost stations FUR and A22 might be influenced by thick sedimentary successions [see *Bachmann et al.,* 1987].

The observed anomaly in v_p/v_s ratios could also be caused by structural effects like topography at the Moho, which is observed beneath the western Eger Rift. *Zandt et al.* [1995] obtained v_p/v_s ratios of 1.62 to 1.64 for the westernmost Basin and Range Province, North America. They discussed the very low values in that region as being possibly caused by the breakdown of the assumption that the crust is laterally homogeneous. A lateral change in crustal thickness of 5 km together with an unchanged Moho conversion time would lead to a v_p/v_s change of 3.5 % (1.67 instead of 1.73) according to *Zandt et al.* [1995]. Direct conversions and multiples sample different paths within the crust. Therefore, lateral variations also might influence the results. The direct Moho conversions sample the Moho about 5 to 10 km away from the station, whereas the crustal multiples sample the Moho over a distance of 5 to 30 km from the station.

B.3.4 Discontinuities of the mantle transition zone

The seismic discontinuities bounding the mantle transition zone in depths of approximately 410 km and 660 km are interpreted as dominantly caused by the isochemical phase transformation of olivine into spinel structure and its final breakdown to perovskite and magnesiowüstite [e.g., *Helffrich and Wood,* 2000; *Lebedev et al.,* 2002] at pressures of approximately 14 GPa and 24 GPa, respectively. Both transformations are temperature dependent, but have opposing Clapeyron slopes [e.g., *Katsura et al.,* 2004; *Fei et al.,* 2004]. This means, if the temperature is higher than normal (e.g., in a plume environment), the '410' should be deeper (higher pressures) and the '660' shallower (lower pressures). Topography of the upper mantle seismic discontinuities seems to be largely uncorrelated at a global scale, and ‘660’ topography is significantly larger in peak-to-peak amplitude according to *Shearer* [2000]. Studies of triplications, of reflected and converted phases are widely used methods to investigate the seismic discontinuities of the mantle transition zone; very common are Ps receiver function studies [e.g., *Kind and Vinnik,* 1988; *Stammler et al.,* 1992; *Petersen et al.,* 1993; *Chevrot et al.,* 1999; *Li et al.,* 2000a, 2003a; *Shearer,* 1991, 2000].

One common approach to study the depth of the upper mantle discontinuities with receiver functions is stacking of the move-out corrected single traces for each station separately, especially for widely spaced stations and short registration periods. As already discussed above, strong converted phases

within 20 seconds delay time are caused by a sedimentary cover (especially beneath the Gräfenberg Array) or velocity gradients in the uppermost crystalline crust, the Moho discontinuity and its multiple phases. About four times weaker (in amplitude) converted phases are visible at 44 to 46 seconds and 67 to 69 seconds delay times (Figure B.8). These phases should be related to the upper mantle discontinuities, as it could be shown in Figure B.1 calculating synthetic receiver functions for relatively simple velocity models. The observed delay times of converted phases from the discontinuities of the mantle transition zone at single stations are listed in Table B.I.

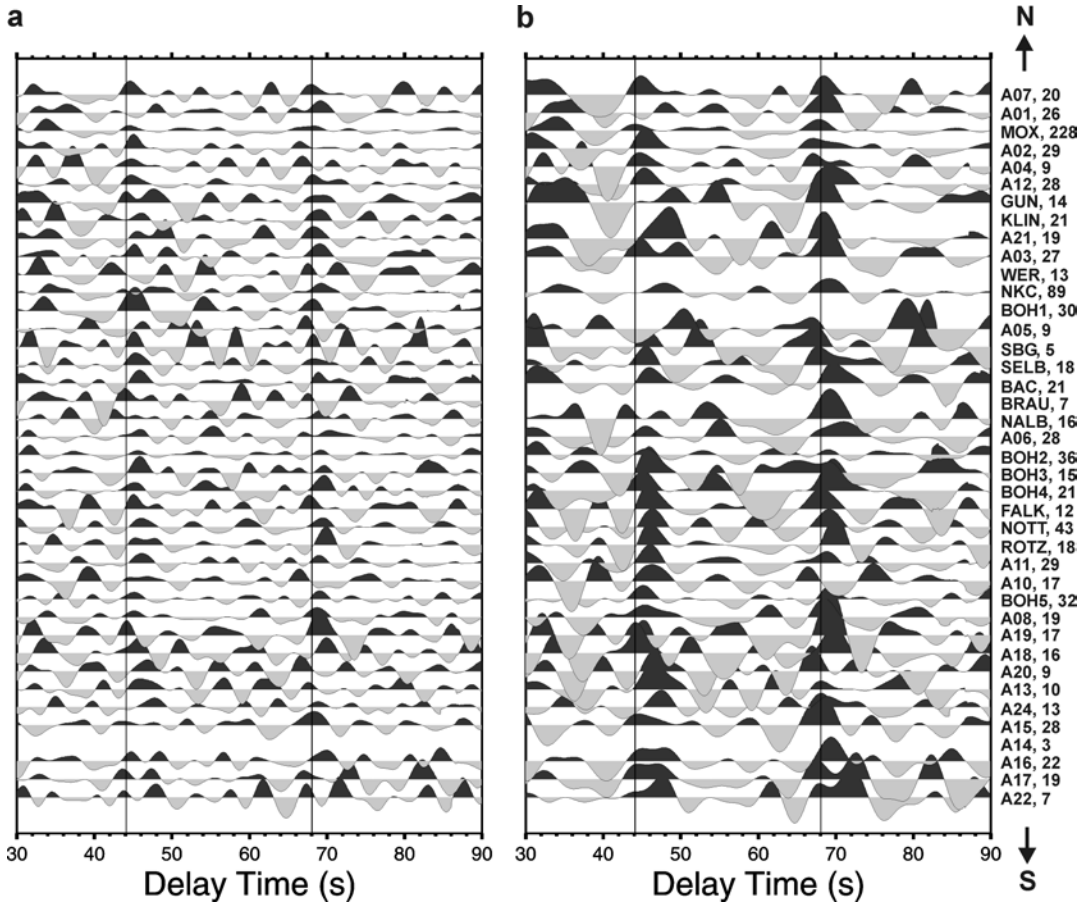

Figure B.8
Stacked move-out corrected (for 67° epicentral distance) traces of the single station analysis of permanent and temporary stations in the western Bohemian Massif. Different band-pass filters were applied **(a)** with corner periods of 3 and 20 seconds, **(b)** with corner periods of 5 and 20 seconds. Theoretical delay times of the '410' and '660' conversions predicted by the IASP91 velocity model [*Kennett*, 1991] are marked by vertical solid lines. An apparent deepening (late arrivals) of the '410' is evident for several stations (see also Table B.I).

Delayed arrival times of the '410' and '660' of up to 2 seconds were observed at many stations in the western Bohemian Massif. The differential travel times for converted phases from the transition zone ($dt_{660\text{-}410}$) are generally about 24±0.5 seconds (see Table B.I; Figure B.8). At some stations, a lower $dt_{660\text{-}410}$ might indicate a real thinning of the transition zone [see *Li et al.,* 2003a], assuming no seismic velocity variations within the transition zone. No indications (coherent phases) for a seismic discontinuity at 520 km depth are observed in this study.

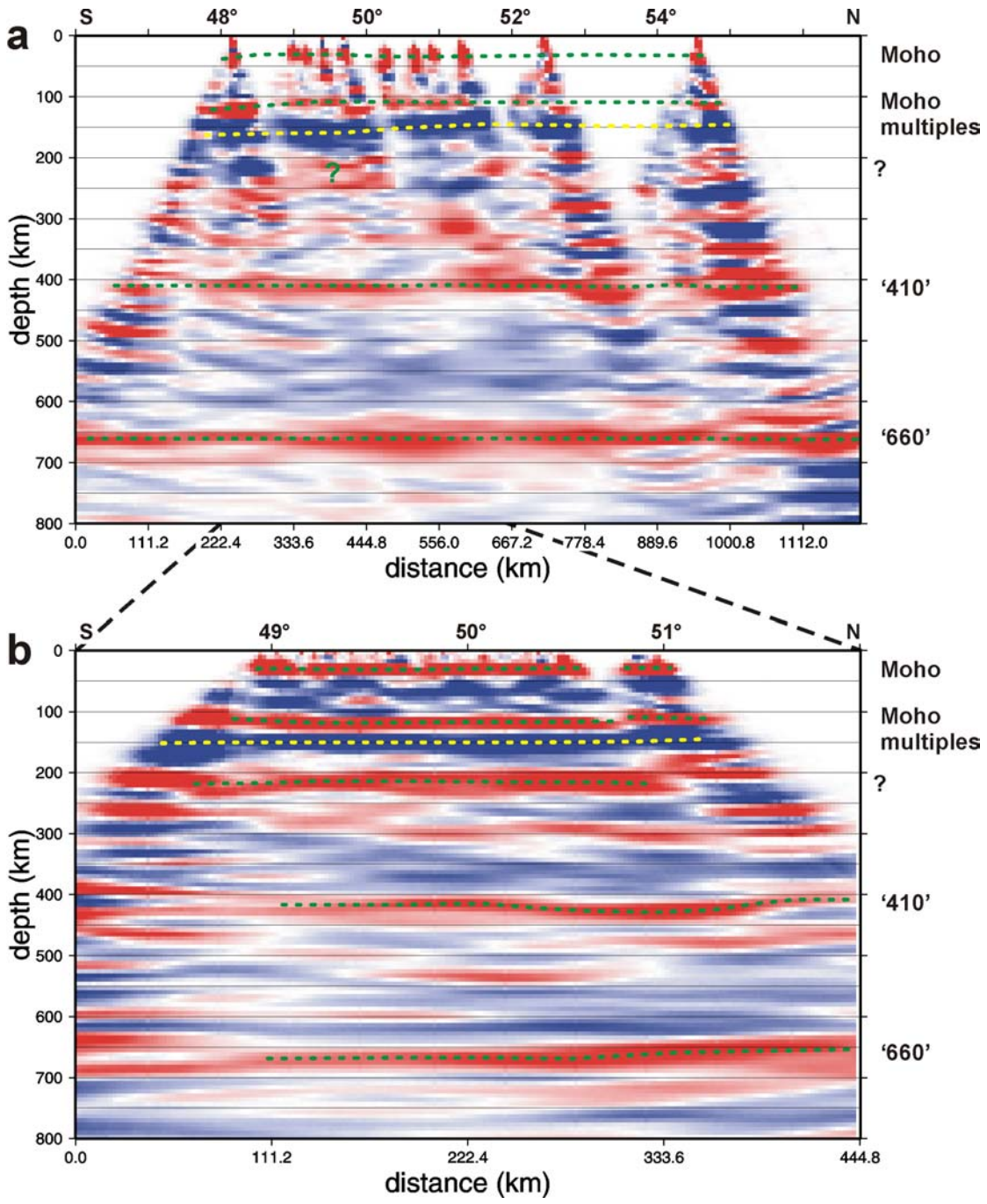

Figure B.9
Migrated sections along 12°E and 12°30'E with data from permanent **(a)** and temporary **(b)** stations in the study area, respectively. For the migrated profile along 12°E teleseismic data from permanent stations FUR, KHC, WET, GRA1, GRB1, GRC1, PRU, NKC, MOX, BRG, CLL, CLZ, BRNL, RUE, and RGN were used and processed in the same way as the data from the temporary stations. Data were provided by the data centres in Erlangen (GRF, GRSN), Potsdam (GEOFON) and Praha (IG CAS). IASP91 seismic velocity model [*Kennett*, 1991] was used for migration.
The apparent deepening of the '410' between 50.5 and 51°N **(b)** is most probably caused by velocity variations in the upper mantle. Delayed '410' conversions are observed at stations further to the south, as it is obvious from Figure B.8. Since most events come from northeastern back-azimuths, the delay is projected towards the north along a N-S profile. However, also a real deepening 'of the 410' cannot be excluded at the present stage of investigation.
A strong phase at about 210 km might be an indication for a seismic discontinuity (like the '220' in PREM; *Dziewonski and Anderson* [1981]) or can be a further multiple phase from the Moho. The later interpretation would imply a generally very strong velocity contrast at the Moho and only small damping of teleseismic waves within the crust.

Figure B.9 shows a north-south migrated section projected along a profile at 12°30'E using data from the temporary networks in the western Bohemian Massif (b) in comparison to a migrated section along 12°E using data from permanent stations in Germany and the Czech Republic (a). For the migration, again the IASP91 velocity model was used. The overall structure is similar for both data sets, including a strong phase in about 200-250 km depth beneath the temporary stations in the western Bohemian Massif, and the discontinuities of the transition zone. North (-east) of the Vogtland/NW-Bohemia area a small-scale deepening of the '410' by about 20 km is indicated.

In my opinion, this apparent deepening is an effect of the upper mantle velocity structure [see also *Kind and Vinnik,* 1988], which is consistent with receiver function modelling (Figure B.1). This is also indicated by the variations in delay times of the '410' recorded at different single stations close to each other (Figure B.8, Table B.I). However, a further detailed analysis (including mapping) of the '410' and '660' discontinuity conversions in the area is necessary. As in the single station analysis, no (coherent) conversions from a seismic discontinuity at 520 km depth could be observed.

B.3.5 Synthetic receiver functions for published crustal seismic velocity models

Synthetic receiver functions calculated for published regional seismic velocity models, using the plane wave approximation, are shown in Figure B.10. The different models resulted from refraction (Figure B.10a-c, e-f) and reflection seismic studies (Figure B.10g-i) as well as from analysis of surface waves (Figure 10d). There are simple models without strong velocity contrast/gradients in the crust, models with a high-velocity lower crustal layer, and with high- or low-velocity layers in the upper to middle crust. For comparison of the synthetic with the observed receiver functions sum traces with (trace V2, bottom) and without the "6 s phase" (trace V1, middle), and receiver functions from a nearby station (top) are shown. It is evident from Figures B.10 and B.4 that relative smooth crustal velocity models can explain most of the observed data whereas complex P-wave models (mainly from reflection seismic studies) with more than one high- or low- velocity layer in the crust do not explain the observed data.

Figure B.10 (next page)
Synthetic receiver functions (solid line) from published regional seismic velocity models. For comparison, observed receiver functions (dashed lines) are shown: the sum traces with (trace V2, bottom) and without the "6 s phase" (trace V1, middle) and sum traces from nearby stations (top). The plane wave approximation [*Kind et al.,* 1995] was used for the calculation. The sum traces of the corresponding L components were used as input P-signal. Scale shown corresponds to 10 % of the amplitude of the primary P-signal. Most of the models can explain at least the primary and multiple Moho phases in the observed receiver functions.

Gräfenberg - *Aichele* [1976]

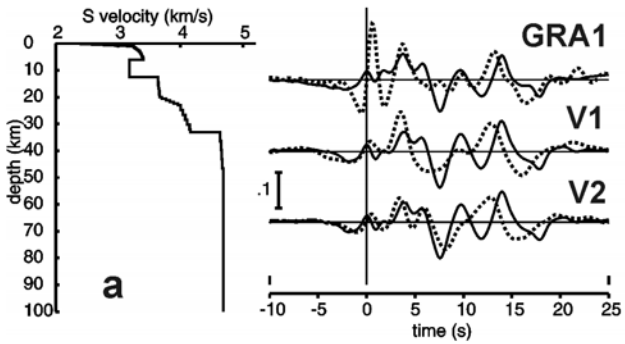

MOKH - *Plešinger et al.* [1994]

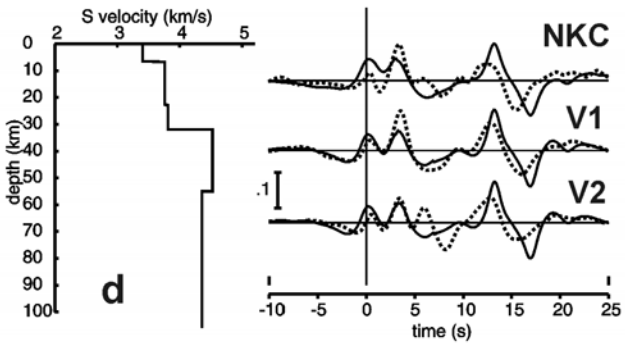

MVE90 CMP1 - *Behr et al.* [1994]

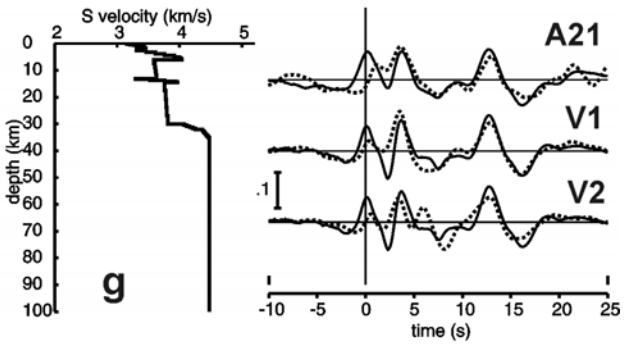

GRANU95 shotpoint F - *Enderle et al.* [1998]

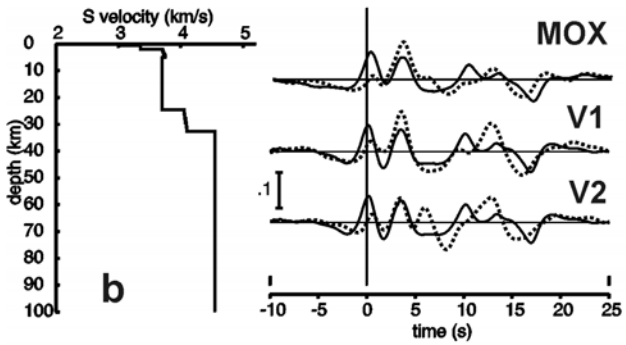

W-Bohemian Massif - *Strößenreuther* [1982]

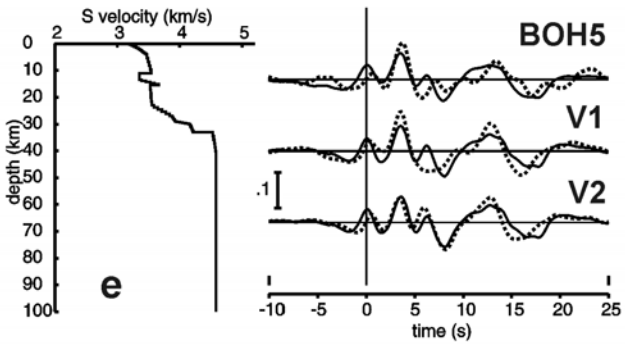

MVE90 CMP2 - *Behr et al.* [1994]

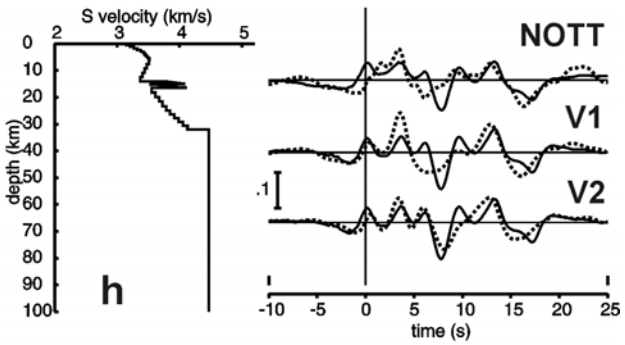

Vogtland - *Köhler et al.* [1989]

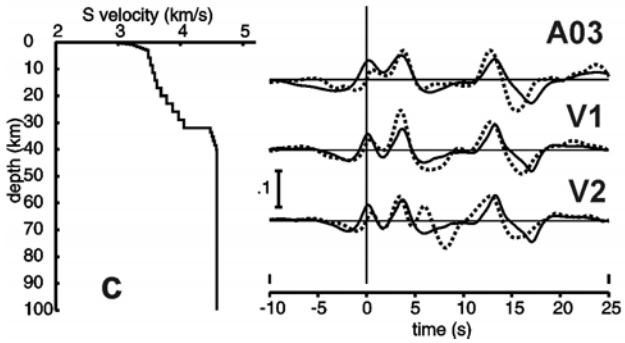

Vogtland - *Schulze and Lück* [1992]

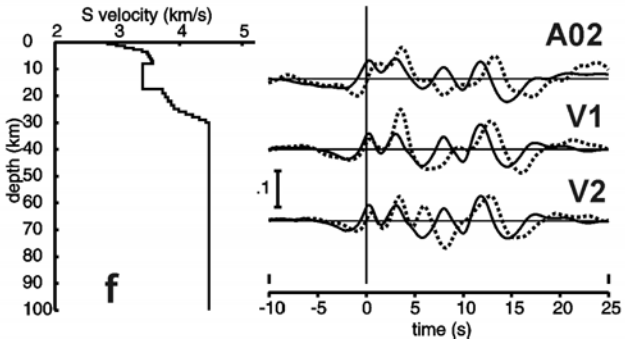

KTB MN - *Schmoll et al.* [1989]

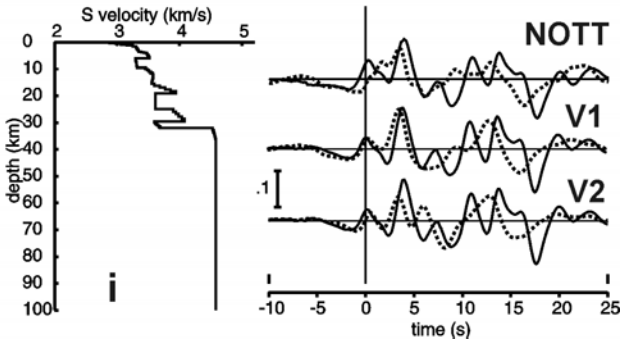

B.3.6 Uncertainties and resolution of the method

Variations depending on recording time and back-azimuth coverage

The vast amount of seismic data from the permanent stations GRA1 (1980-1997) and MOX (1993-1997) was studied in more detail to estimate the uncertainties of the results due to short recording periods at temporary stations. The Moho depth, v_p/v_s ratio, and Moho Ps delay time were analysed for different time spans (from 2 months up to 18 years) and for different back-azimuths, respectively (Figure B.11; Table B.III). From Figure B.11 it is obvious that several tens of traces are needed to obtain a stable result. Typically, this requires at least one year of recording time. The inverted Moho depths and v_p/v_s ratios can vary for short time spans (only few events) by up to 2 km and 0.05, respectively. The crustal thickness and v_p/v_s ratio may depend on the back-azimuth of teleseismic events, and therefore, also on the back-azimuth distribution of seismic events at the stations. The values obtained vary by up to 2 km for crustal thickness and 0.07 for v_p/v_s ratio at the two stations GRA1 and MOX for different back-azimuths. These variations might be caused by real Moho topography around the stations, and therefore they are not considered as an error of the method. Because there is no perfect back-azimuth coverage for most of the temporary stations, the data were stacked over all back-azimuths. This way, an average crustal thickness beneath each station was obtained.

Uncertainty of the grid search method and Ps delay time measurements

One can estimate an error of the grid search if one assumes that all stacks in the crustal thickness-v_p/v_s ratio domain within the 95 % contour of the maximal stacked amplitude are possible solutions (white areas in Figure B.6). This procedure results in estimated errors for the average values of v_p/v_s ratios and crustal thicknesses of ±0.08 and ±1.5 km, respectively (Table B.I). A systematic error also could exist due to the assumed average crustal P-wave velocity of 6.3 km/s. Lateral variations of the average P-wave velocity within rifts and at terrane boundaries might exist. If one assumes a higher P-wave velocity of about 6.5 km/s, as it might be the case for the central Bohemian Massif, then the Moho depth increases by about 2 km. If one assumes 6.0 km/s, the values decrease by about 2 km. In this analysis, v_p/v_s ratios vary by about 0.03, but show no direct dependence on P-wave velocity. Up to now, there is no information available on small-scale average seismic velocity variations in the region. That's why a constant value was used. Also, I do not think that the average crustal P-wave velocity varies over short distances by more than 0.2 km/s. Therefore, the observed variations in Moho depth do probably not depend significantly on crustal P-wave velocity in the region under study. However, a linear trend to underestimated Moho depths might exist towards the central Bohemian Massif.

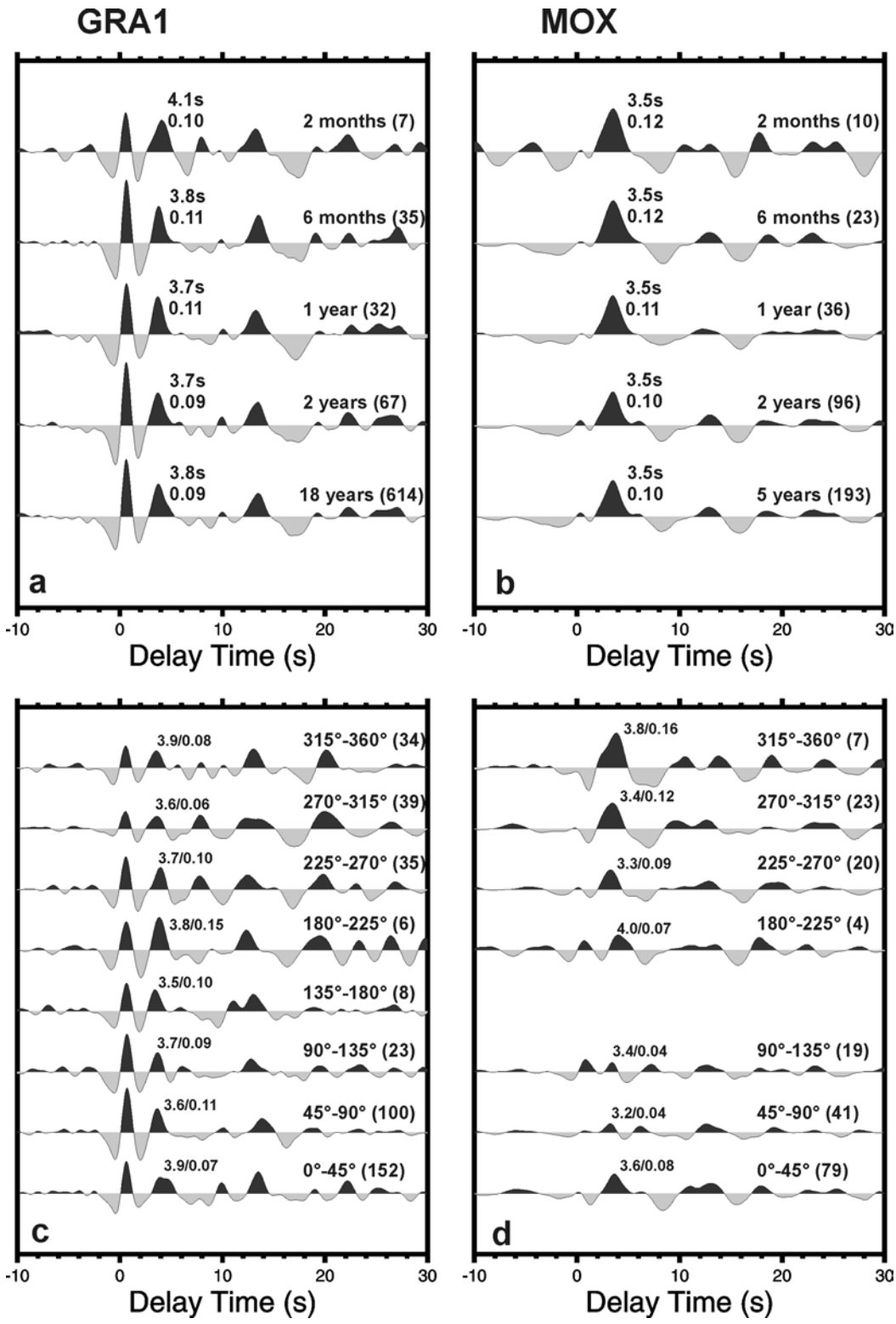

Figure B.11
Stacked receiver functions from stations GRA1 and MOX from different time spans **(a, b)** and back-azimuths **(c, d)**. The numbers to the right of the time spans or back-azimuth windows indicate the number of stacked traces. Traces were high-pass filtered with 20 seconds corner period and move-out corrected before stacking. The numbers at the converted phase from the Moho represent the observed delay times and the relative amplitude ratios SV/P (amplitude of the converted phase on the SV/Q component after deconvolution with the P wave signal on the L component). Only small variations of the waveform were observed for the different time spans except for that of only 2 months, both at GRA1 and MOX **(a, b)**. Note that there are only small variations of the Moho conversion at station GRA1 with back-azimuth **(c)**, whereas there are strong variations at station MOX **(d)**. It seems that a complex Moho structure (branching) exists northeast of MOX.

The delay times of the direct Ps-converted phase and its multiples from the Moho were re-calculated using the Moho depths and v_p/v_s ratios from Table B.I, and an average crustal P-wave velocity of 6.3 km/s. The obtained values show a good agreement with the observed data (Figure B.4). This indicates that the method works well, at least at stations with a more or less simple velocity structure and clear primary and multiple Moho conversions.

Analysing 18 years of data from station GRA1 (1980-1997) for each year separately, variations in the Moho Ps delay times of 0.1 to 0.2 seconds could be observed (see Figure B.12, Table B.III). Therefore, the uncertainty of Moho Ps delay time measurements for temporary stations, which were operated for one year, might also be in the range 0.1 to 0.2 seconds. Delay times t_{p410s} and t_{p660s} observed in station stacks of GRA1 for different years of observation vary by about 0.5 to 1.0 seconds, showing no dependency on the filter used. Therefore, it can be assumed that the uncertainty for delay time measurements of conversions from the mantle transition zone ('410' and '660') are in the range of 0.5 to 1.0 seconds also for the temporary stations.

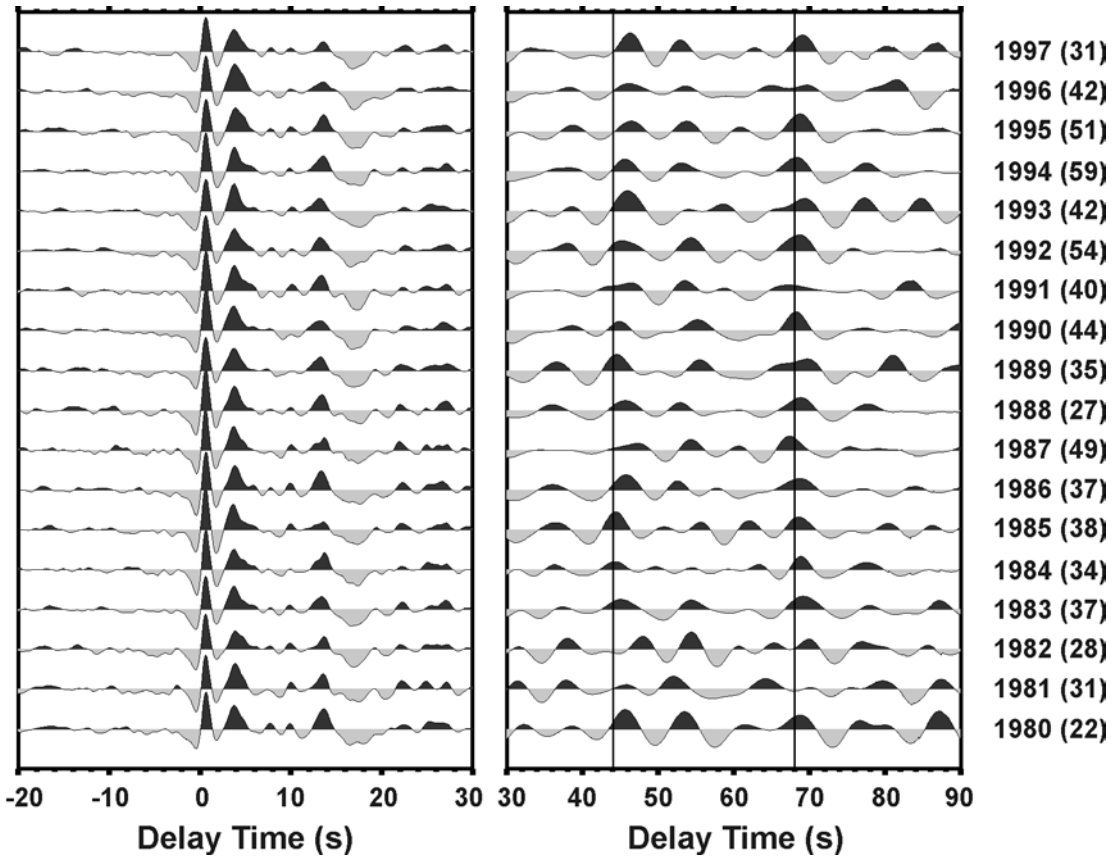

Figure B.12
Stacked receiver functions from stations GRA1 for every year between 1980 and 1997. The numbers to the right of the year indicate the number of stacked traces. Data were high-pass filtered with 50 seconds corner period in the time range -20 to 30 seconds delay time and band-pass filtered (corner periods 5 to 50 seconds) from 30 to 90 seconds delay time, respectively (see also Table B.III).

Summarizing, the maximum uncertainty for the observation of variations in the average crustal thickness ΔH is ±1.5 to ±2 km, and for v_p/v_s ratio ±0.08. The uncertainty of Moho Ps delay time measurements is in the range 0.1 to 0.2 seconds, which results also in about ±1.5 km for crustal thickness variations. The uncertainty of Ps delay time measurements for the '410' and '660' in single station stacks is about 0.5 to 1.0 seconds.

Table B.III. Variations of Ps delay times (Moho, '410', '660'), crustal thickness H, and average crustal v_p/v_s ratio at station GRA1 for the years 1980-1997. Data from each year were analysed separately in comparison to the whole data set.

	HP 20s			HP 50s	relative	BP 3s-20s			BP 5s-20s			
Year	v_p / v_s	H (km)	t_{PMs} (s)	t_{PMs} (s)	amplitude	t_{P410s} [s]	t_{P660s} [s]	$dt_{660-410}$ [s]	t_{P410s} [s]	t_{P660s} [s]	$dt_{660-410}$ [s]	n
1980	1.71	32.0	3.7	3.7	0.10	45.2	68.8	23.6	45.7	68.7	23.0	22
1981	1.76	31.0	3.9	3.9	0.11	45.5	69.1	23.6	45.8	(67.2)	21.4	31
1982	1.74	31.5	3.8	3.9	0.08	48.5	69.7	21.2	48.0	69.9	21.9	28
1983	1.73	31.5	3.7	3.7	0.10	45.0	69.0	24.0	45.1	69.1	24.0	37
1984	1.72	32.0	3.7	3.7	0.09	45.0	69.0	24.0	44.3	68.8	24.5	34
1985	1.68	32.5	3.6	3.6	0.11	44.7	(68.9)	24.2	44.4	68.5	24.1	38
1986	1.74	31.5	3.8	3.8	0.10	45.1	68.8	23.7	45.8	68.7	22.9	37
1987	1.71	32.0	3.7	3.7	0.10	45.7	67.2	21.6	47.3	67.4	20.1	49
1988	1.75	31.5	3.8	3.8	0.10	46.0	69.2	23.2	45.7	68.8	23.1	27
1989	1.73	31.5	3.7	3.7	0.09	44.7	68.2	23.5	44.5	69.7	25.2	35
1990	1.71	31.5	3.7	3.7	0.10	45.0	68.3	23.3	44.9	68.2	23.3	44
1991	1.73	31.5	3.8	3.8	0.11	47.2	68.4	21.2	46.4	67.3	20.9	40
1992	1.73	31.5	3.8	3.8	0.09	44.2	69.4	25.2	45.1	68.7	23.6	54
1993	1.74	31.0	3.7	3.7	0.11	45.6	68.8	23.2	46.0	69.3	23.3	42
1994	1.74	31.5	3.8	3.8	0.10	45.4	69.1	23.7	45.6	68.3	22.7	59
1995	1.74	31.5	3.9	3.9	0.10	45.1	69.2	24.1	46.5	68.7	22.2	51
1996	1.75	31.5	3.8	3.8	0.12	45.6	69.3	23.7	46.1	69.6	23.5	42
1997	1.72	31.5	3.7	3.8	0.09	46.4	69.4	23.0	46.3	69.1	22.8	31
Mean	**1.73**	**31.6**	**3.8**	**3.8**	**0.10**	**45.5**	**68.9**	**23.3**	**45.8**	**68.7**	**22.9**	**39**
σ	0.02	0.4	0.1	0.1	0.01	1.0	0.6	1.0	0.9	0.8	1.2	
1980-1997	**1.73**	**31.5**	**3.7**	**3.8**	**0.10**	**45.0**	**68.9**	**23.9**	**45.7**	**68.7**	**23.0**	**701**

Another problem is the use of short period data without clear crustal multiples, especially at the WEBNET and KRASNET stations (Figure B.5). For the stations from these networks, crustal thicknesses were calculated from the observed Moho Ps delay times using v_p/v_s ratios from adjacent broadband stations. Unfortunately, the stations from the short-period networks were operated in a triggered mode, and the length of the time windows used for deconvolution is sometimes very small (only about 20 seconds). At station NKC, data from a broadband and a short-period seismometer were analysed, but from different time intervals (Tables B.I and B.II; Figures B.4 and B.5). At another site (nearby stations A03 and WER; Figure B.4, Table B.I) two different seismometers were operated at different times. For both locations, similar results could be obtained using different instruments.

B.4 Geophysical indications for Moho updoming and the origin of the "6 s phase"

B.4.1 Local Moho updoming beneath the western Eger Rift

In this section, the discussion of Moho depth variations is focused on the area of swarm-earthquakes, active mantle degassing, and Quaternary volcanism in the Vogtland/NW-Bohemia region. The local Moho depth distribution is plotted in Figure B.13, including the results from the short period stations that are not plotted in Figure B.7. Moho depths at short period stations are computed using v_p/v_s ratios of neighbouring broadband stations. Crustal thickness beneath the western Eger Rift is only about 27 km, whereas it is about 31 km in the surroundings. It is clear from the discussion of uncertainties above, that the observed updoming beneath the western Eger Rift is near the observation limit at a single station. Because different independent stations show an updoming in this area, in the Ps delay times (up to 0.8-1.0 seconds) as well as in the inverted Moho depths (about 4 km), I think that the observation is real. It is unlikely that errors in one region point always in the same direction, they should scatter.

Moho updoming seems to be restricted to the crossing of the Eger Rift and the Regensburg-Leipzig-Rostock Lineament (Cheb Basin; Figures A.1, B.13), however, there is no control (data) on the situation further to the northeast. To the southwest, no decreased Moho depths can be observed beneath the continuation of the Eger Rift. The area, where an updoming of the Moho is observed, has an NNW-SSE extension of approximately 40 km. The top of this Moho antiform is located beneath the gas escape centre Františkovy Lázně/Cheb Basin (section A.2.4; Figures A.4, B.13).

Moho updoming beneath continental rifts is nothing unusual, and it is observed beneath the southern Upper Rhine Graben [*Prodehl et al.,* 1995], the French Massif Central [*Zeyen et al.,* 1997], the Rio Grande Rift [*Baldridge et al.,* 1995], and the Kenya Rift [*Braile et al.,* 1994]. It seems to be a common structural feature of graben systems. However, there seems to exist also strong variations in Moho

depths along the axial grabens, as in the case of the Kenya Rift [*Mechie et al.,* 1994a]. One important feature in the western part of the Eger Rift is the local scale overlapping of Moho updoming with upper mantle derived gas exhalations and Quaternary volcanism (Figure B.13).

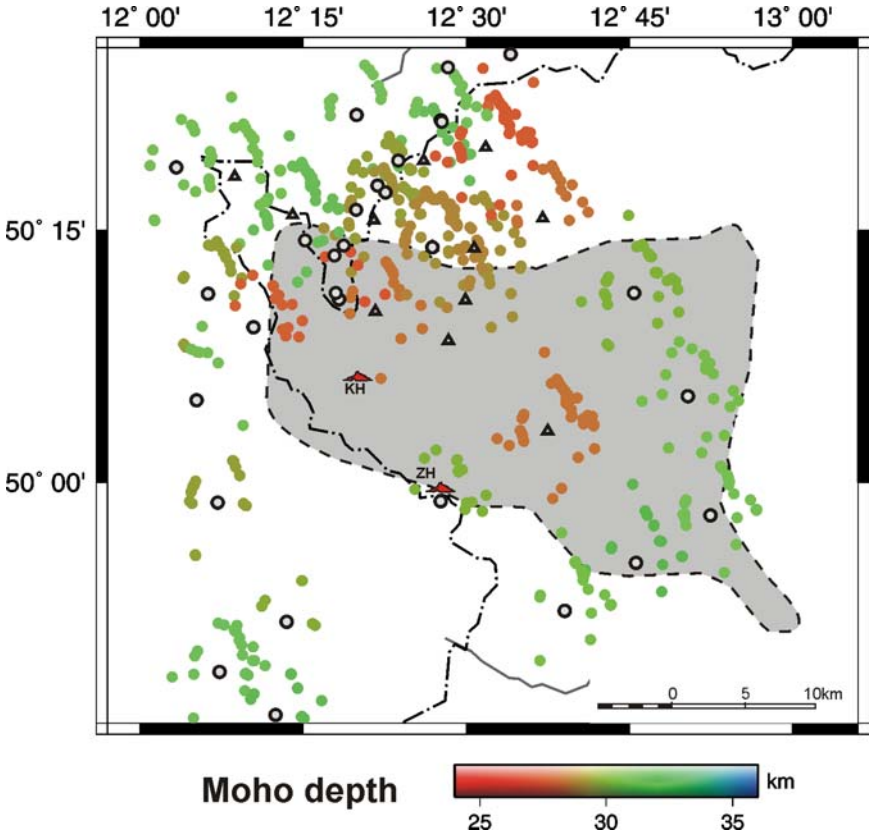

Figure B.13
Comparison of the Moho depths and the results of gas geochemical investigations (see Figure A.4). This map also contains the calculated Moho depths for the short period stations (see Table B.II).
Grey: CO_2 emanation area; KH – Komorní Hůrka, ZH – Železná Hůrka.

At the broadband station BOH1 within the Eger Rift, no clear Moho Ps conversions (Figure B.3) could be observed, mainly in the NE-back-azimuths (0-45°, Figure B.13). This points to a broad gradient zone, strong lateral heterogeneity at Moho level, or an inclination of the crust-mantle boundary in this area. Similar observations were also made at other stations (BOH2, SELB, NALB, KLIN, and GUN) associated with the find of a converted phase at about 6 seconds delay time, possibly stemming from beneath the Moho. In the case of BOH1 the area with the "diffuse" Moho character correlates well with the reflection free part in the 9HR seismic profile [*Tomek et al.,* 1997]. The reflection free parts might be caused by „bad“ shots and industrial noise in the Sokolov Basin, a lignite mining area [*Tomek,* personal communication]. *Behr et al.* [1994] also found indications for a disturbed Moho with variations of 2 to 3 km beneath the Western Eger Rift. Offline observations of shots along the MVE’90 seismic profile indicate that the Moho is shallower beneath the Cheb Basin than further to the northeast beneath the Sokolov Basin [Figure 2.16 in *Behr et al.,* 1994].

Wilson et al. [2003] observed similar diffuse Moho conversions at stations above the Coso geothermal area, California. In their case, the converted phases seem to be strongly influenced by a magmatic system within the upper crust. No strong geothermal anomaly or magmatic system seems to exist in the upper crust beneath the Vogtland/NW-Bohemia area, with the exception of the Karlovy Vary Spa area. Hot springs in this area are attributed to a highly radiogenic Variscan granite complex (Karlovy Vary pluton) [see *Förster and Förster,* 2000]. Therefore, I conclude that the diffuse and weak Moho conversions really show effects at the crust-mantle boundary beneath the region.

B.4.2 The origin of the "6 s phase" – conversions from subcrustal depths or multiples from an intracrustal layer?

Clear converted phases with delay times of about 6 seconds are observed at stations SELB, NALB and NKC (Figure B.3, light arrows). Indications for such a phase were also found near stations BAC, BOH2, LAC, KLIN and GUN. The study area was divided into several boxes, and a common conversion point method was applied to search for the spatial distribution of the "6 s phase" (Figure B.14). The size and distribution of the boxes was chosen after several tests, including stacking within back-azimuth windows at single stations.

Receiver function modelling

To check the origin of the "6 s phase", synthetic receiver functions were calculated (Figure B.15) using the plane wave approximation [*Kind et al.,* 1995]. At first, a model with a more or less simple crustal structure is modelled, which can explain the data without the "6 s phase" (Figure B.15a). Subsequently, single low- or high seismic velocity layers were added into the crust and uppermost mantle. The response of each model is compared to the observed receiver functions, the sum of all traces without a "6 s phase" (trace V1, top) and with a "6 s phase" (trace V2, bottom).

Indications for low velocity channels in the middle crust as modelled in Figure B.15b were observed by several active seismic measurements [e.g., *Knothe*, 1972; *Ströβenreuther*, 1982; *Holbrook et al.,* 1988; *Behr et al.,* 1994]. This relative simple model shows the best fit with the observed data up to 25 seconds delay time. Further tests showed that a low velocity channel (about 2 km thick, depth 11-13 km) within the crust cause multiples at about 6 seconds delay time. The velocity reduction could be due to lithological contrasts (e.g., quartzite) or due to the presence of fluids. Assuming a constant v_p/v_s ratio for the whole crust, velocities are reduced both by 8 % (5.7 instead of 6.2 km/s for v_p). In a fluid-rich layer the v_p/v_s ratio might be increased. *Faul et al.* [1994] published values for the velocity reduction per 1 % melt or fluid distributed in thin, elongated inclusions or within triple junction

tubules (1 to 1.8 % for v_p, 2.3 to 3.3 % for v_s). If I assume that these values obtained for basic to ultrabasic melt inclusions at upper mantle conditions are also more or less valid for a mid-crustal regime, the observed data could be modelled as an intracrustal layer filled with 3 to 5 % fluids. In this case, the v_p/v_s ratio is about 1.87 (velocity reduction: 5 % for P-waves, 11.5 % for S-waves). The lateral extension of such low-velocity zones should be at least 5 km, because only in this case multiple phases would be observed.

High velocity layers within the crust (Figure B.15c) might represent geologic bodies comparable to the "Erbendorf body", which is postulated beneath the KTB [*DEKORP*, 1988; *Emmermann and Lauterjung*, 1997]. The fit between synthetic and observed receiver functions in the first 6 seconds is not as good as for the other models, indicating that it might not be the most realistic model.

Model d (Figure B.15d) shows a hypothetic single thick magma reservoir in a "normal" upper mantle, assuming about 5 to 7 % magma dispersed in a more than 5 km thick layer within the lithosphere. Velocities are reduced by about 9 % (P-waves) and 16.5 % (S-waves; v_p/v_s equals 1.95), respectively, according to the maximum values published by *Faul et al.* [1994]. Model d does not fit the observed data at delay times greater than 14 seconds. If this low velocity anomaly would be a widespread phenomenon (channel) and no anelastic damping or scattering exist (as it is assumed by the modelling) one would expect to observe the strong multiple phases from this layer in the real data. However, if the anomaly is only a local phenomenon with a lateral extension of less than 25 to 30 km, or there exist strong damping and scattering, no multiple phases would be observed.

Model e (Figure B.15e) shows a (relative) high-velocity layer between upper mantle with reduced P- (S-) wave velocities compared to the IASP91 reference model (7.6 km/s above and 7.8 km/s below instead of 8.2 km/s). The discontinuities in the upper mantle can also be modelled as sharp boundaries. A sharp discontinuity in about 50 km depth produces a strong multiple phase at 20 seconds delay time in the synthetic traces, whereas a gradient zone at that depth range produces only a weak multiple, which might be not observable in the real data due to damping and scattering. These models might represent some eclogitic bodies within a "normal" uppermost mantle or a layer of "normal" mantle in-between "fluidised" mantle. Reduced seismic velocities in the upper mantle and an uplift of the asthenosphere were reported from surface wave studies [*Plešinger et al.,* 1994; *Passier and Snieder*, 1996] and studies of P-residuals [*Plomerová et al., 1988; Plomerová and Babuška,* 1998].

In all models discussed above (Figure B.15), it is necessary to introduce a broad gradient zone in the lower crust and at the Moho instead of a sharp velocity contrast to fit the amplitudes of the observed Moho conversions. Because the modelled sum trace is the result of stacking data from stations with different Moho depths, the contrast and therefore the amplitudes of conversions are damped. However, observations of very weak (in amplitude) conversion at several single stations (e.g., BOH1, SELB; Figure B.3) in the CO_2 degassing area might indicate the local presence of a gradient zone rather than a sharp (1st order) seismic discontinuity.

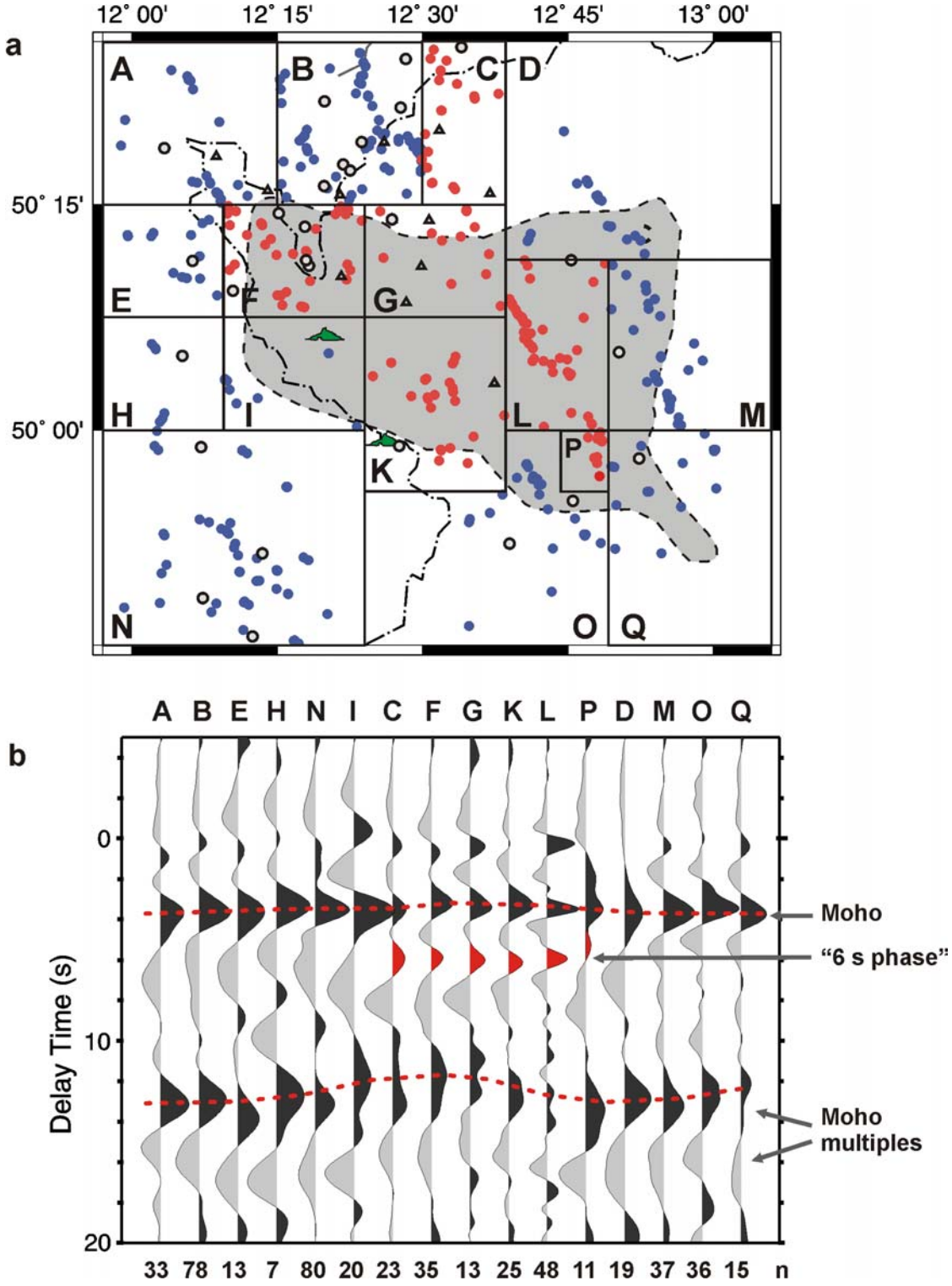

Figure B.14
(a) Distribution of piercing points at 50 km depth. Receiver functions with common conversion points were stacked in each box A-Q **(b)**. Blue dots mark boxes without a "6 s phase". Red dots mark boxes with the "6 s phase". Latter ones correlate with the distribution of mantle-dominated CO_2 emanation vents at the surface (grey shading, see also Figure A.4). Green triangles: locations of the two Quaternary scoria cones.
For the mapping of the "6 s phase" data from short period stations, which are mostly located in the main epicentral area, are included. Therefore, the signals from the Moho and the "6 s phase" contain higher frequencies than the traces in the surrounding area. The radius of the first Fresnel zone at 50 km depth, which can be used as an approximation for lateral resolution, is about 20 km. Note that the Quaternary volcanoes are located at the western edge of the red "6 s region". The Moho updoming beneath the central study area is obvious from the stack traces in **(b)**, especially looking at the first Moho multiples.

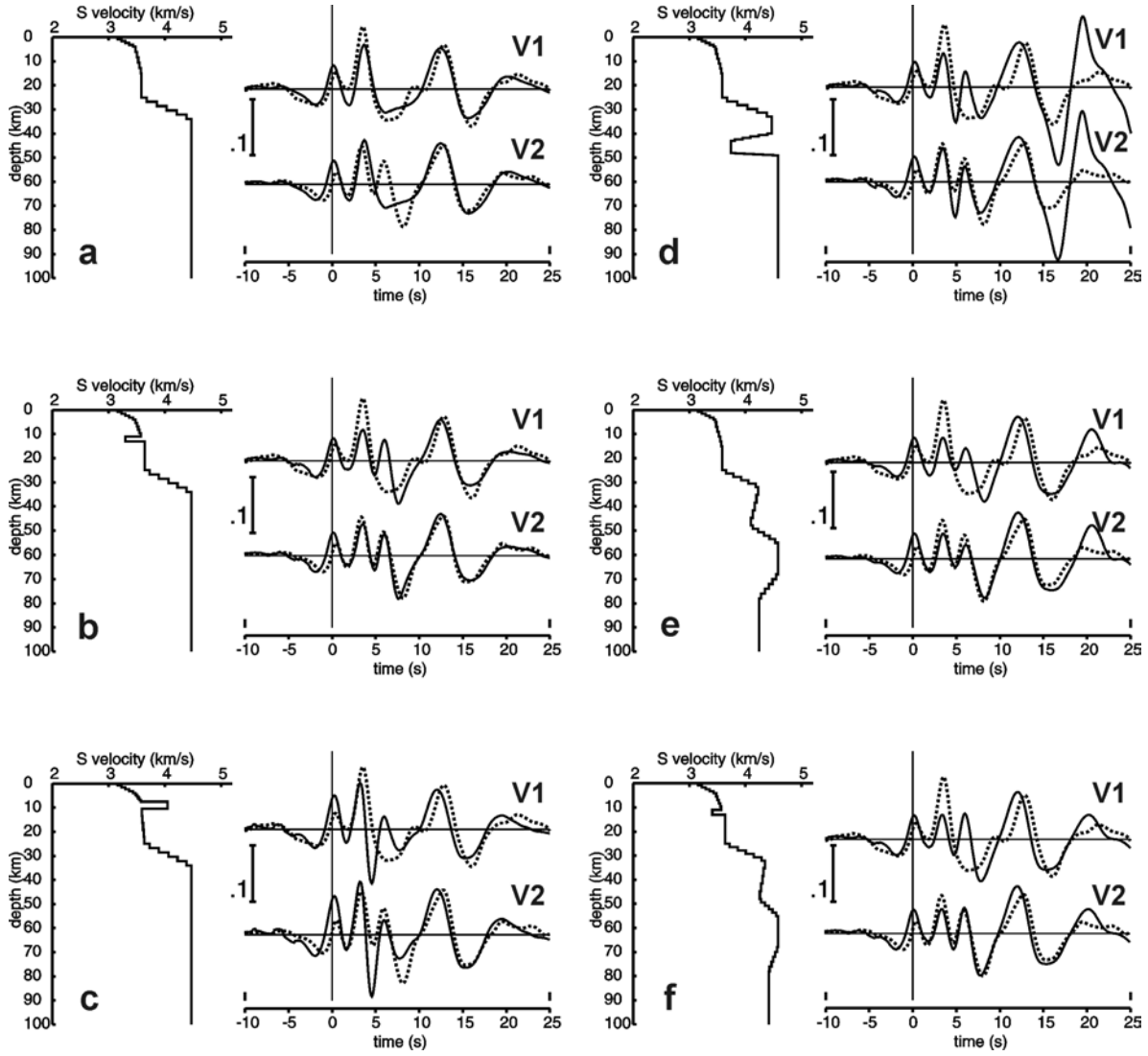

Figure B.15
Forward modelling of observed receiver function waveforms for a number of relative simple models (model response shown by solid lines). V1 – stack of all traces without the "6 s phase" in Figure 8, V2 – stack of all traces with the "6 s phase" (data shown by dashed lines). Plane wave approximation [*Kind et al.,* 1995] was used. The input P-signal is the sum of the corresponding L traces. The scale gives the portion of primary deconvolved P signal, that means Moho Ps conversions are about 10 % in amplitude of the incoming P-wave.
Model **a** shows a simple crustal structure with a gradient zone at Moho depths. This simple model cannot explain the observed phase at 6 seconds delay time. Model **b** shows the effect of a low velocity layer in the upper-middle crust between 11 and 13 km. This depth range corresponds to the base of the seismogenic zone in the area. The model is similar to that of *Strößenreuther* [1982] from the Bavarian forest. Model **c** simulates a high-velocity layer in the upper crust (7.5 to 10.5 km depth). High velocities might be indicative for equivalents of the postulated "Erbendorf body" further to the west [*DEKORP,* 1988; *Emmermann and Lauterjung,* 1997]. Model **d** represents a hypothetic thick magmatic layer in the upper mantle with about 5 to 7 % melt content and a velocity reduction of up to 9 % for v_p and 16.5 % for v_s, according to *Faul et al.* [1994]. Model **e** simulates a high velocity layer in the upper mantle. "High velocity" is relative: the layer could represent a real high velocity layer in a "normal" upper mantle or a layer of "normal" mantle in-between mantle with reduced seismic velocities. Results from surface wave studies [*Plešinger et al.,* 1994; *Passier and Snieder,* 1996] argue for the latter case. Model **f** represents a combination of models b and e with reduced amplitudes (50 %) of each velocity anomaly.